Vol. 92 No. 1 pp. 183–209 ACTA GEOLOGICA SINICA (English Edition) Feb. 2018

Platinum-Group Elements Geochemistry and Chromian Spinel Composition in Podiform Chromitites and Associated Peridotites from the Cheshmeh-Bid Deposit, Neyriz, Southern Iran: Implications for Geotectonic Setting

Batoul TAGHIPOUR* and Farhad AHMADNEJAD

Department of Earth Sciences, Faculty of Science, Shiraz University, Shiraz, Iran 71454

Abstract: Dunite and serpentinized harzburgite in the Cheshmeh-Bid area, northwest of the Neyriz ophiolite in Iran, host podiform chromitite that occur as schlieren-type, tabular and aligned massive lenses of various sizes. The most important chromitite ore textures in the Cheshmeh-Bid deposit are massive, nodular and disseminated. Massive chromitite, dunite, and harzburgite host rocks were analyzed for trace and platinum-group elements geochemistry. Chromian spinel in chromitite is characterized by high $Cr^{\#}$(0.72−0.78), high $Mg^{\#}$(0.62–0.68) and low TiO_2 (0.12 wt%−0.2 wt%) content. These data are similar to those of chromitites deposited from high degrees of mantle partial melting. The $Cr^{\#}$ of chromian spinel ranges from 0.73 to 0.8 in dunite, similar to the high-Cr chromitite, whereas it ranges from 0.56 to 0.65 in harzburgite. The calculated melt composition of the high-Cr chromitites of the Cheshmeh-Bid is 11.53 wt%–12.94 wt% Al_2O_3, 0.21 wt%–0.33 wt% TiO_2 with FeO/MgO ratios of 0.69−0.97, which are interpreted as more refractory melts akin to boninitic compositions. The total PGE content of the Cheshmeh-Bid chromitite, dunite and harzburgite are very low (average of 220.4, 34.5 and 47.3 ppb, respectively). The Pd/Ir ratio, which is an indicator of PGE fractionation, is very low (0.05–0.18) in the Cheshmeh-Bid chromitites and show that these rocks derived from a depleted mantle. The chromitites are characterized by high-$Cr^{\#}$, low Pd + Pt (4–14 ppb) and high IPGE/ PPGE ratios (8.2–22.25), resulting in a general negatively patterns, suggesting a high-degree of partial melting is responsible for the formation of the Cheshmeh-Bid chromitites. Therefore parent magma probably experiences a very low fractionation and was derived by an increasing partial melting. These geochemical characteristics show that the Cheshmeh-Bid chromitites have been probably derived from a boninitic melts in a supra-subduction setting that reacted with depleted peridotites. The high-Cr chromitite has relatively uniform mantle-normalized PGE patterns, with a steep slope, positive Ru and negative Pt, Pd anomalies, and enrichment of PGE relative to the chondrite. The dunite (total PGE = 47.25 ppb) and harzburgite (total PGE =3 4.5 ppb) are highly depleted in PGE and show slightly positive slopes PGE spidergrams, accompanied by a small positive Ru, Pt and Pd anomalies and their Pd_n/Ir_n ratio ranges between 1.55–1.7and 1.36−1.94, respectively. Trace element contents of the Cheshmeh-Bid chromitites, such as Ga, V, Zn, Co, Ni, and Mn, are low and vary between 13–26, 466–842, 22−84, 115–179, 826–−1210, and 697–1136 ppm, respectively. These contents are compatible with other boninitic chromitites worldwide. The chromian spinel and bulk PGE geochemistry for the Cheshmeh-Bid chromitites suggest that high-Cr chromitites were generated from Cr-rich and, Ti- and Al-poor boninitic melts, most probably in a fore-arc tectonic setting related with a supra-subduction zone, similarly to other ophiolites in the outer Zagros ophiolitic belt.

Key words: Cheshmeh-Bid Chromitite, trace elements, platinum-group elements, boninitic magma, supra-subduction zone

* Corresponding author. E-mail: Taghipour@shirazu.ac.ir

1 Introduction

The genesis of podiform chromitites, particularly their content of platinum-group elements (PGE) and tectonic setting of emplacement, is one of most interesting geochemical subjects for recent scientific research (Uysal et al., 2007; Ahmed et al., 2009, 2012; Ismail et al., 2010; Jennessary et al., 2012; Ahmed and Habtoor, 2015; Yang et al., 2015; Robinson et al., 2015; Xu et al., 2015; Xiong et al., 2015a, 2015b; Guolin et al., 2016; Habtoor et al., 2017; Economou-Eliopoulos et al., 2017) However, the factors that control the distribution, textures, and compositions of podiform bodies are still unclear. Podiform chromitites in ophiolites should reflect multi-stage processes involving subduction of lithospheric slabs into the transition zone, crystallization of chromian spinel and some massive chromite at depth, incorporation of ultra-high-pressure (UHP) minerals and highly reduced phases into the chromitites, and entrapment of oceanic lithospheric slabs above subduction zones where they undergo varying degrees of reaction with hydrous, SSZ melts (Robinson et al., 2015; Xiong et al., 2015a, 2015b, 2017; Xu et al., 2015; Yang et al., 2015).

The mineral chemistry of primary chromite and the associated interstitial primary silicate minerals, as well as their order of crystallization, reflects the composition of the parental melt (Rollinson, 2008; Ismail et al., 2010). Compositionally, different types of chromitites in single ophiolitic massifs have been recognized, which can be divided into high-Cr types [$Cr^{\#}$>0.60 where $Cr^{\#}$ is the atomic ratio Cr/(Cr + Al)] and high-Al types ($Cr^{\#}$<0.60) (González-Jiménez et al., 2011; Zaccarini et al., 2011; Xiong et al., 2017). It is believed that high-Cr and high-Al chromitite types are formed from boninitic and MORB-like tholeiitic magmas, respectively (Zhou and Robinson, 1994; Arai and Yurimoto, 1994; Ismail et al., 2014). Podiform chromitite have been regarded as possible sources for PGE (Uysal et al., 2007). Despite Pt, Pd, and Rh (Pd-subgroup), the PGE content of chromitites exhibits a sub-economical enrichment in Os, Ir and Ru (Ir-subgroup). High-Cr chromitites generally have higher PGE contents compared to high-Al chromitites (Gervilla et al., 2005; González-Jiménez et al., 2011; Uysal et al., 2007, 2009), and the differences in the PGE concentration of chromitites depend on the nature of parental melts (Uysal et al., 2009; González-Jiménez et al., 2011; Zaccarini et al., 2011; Kozlu et al., 2014; Economou-Eliopoulos et al., 2017). Based on their melting temperatures, the platinum-group elements are classified into two groups: the Pd-subgroup (PPGE; melting temperature <2000°C) consists of Rh, Pt and Pd and the Ir -subgroup (IPGE >2000°C) consists of Os, Ir and Ru (Kozlu et al., 2014).

A number of podiform chromitite deposits occur in the ophiolites of Iran and have been the focus of several studies (e.g. Rajabzadeh et al., 1998; Jannessary et al., 2012, Shafaii Moghadam et al, 2014, Shafaii Moghadam et al., 2015, Najafzadeh and Ahmadipour, 2016, Zaeimnia et al., 2017, Peighambari et al., 2016). The major element and Platinum-group Element (PGE) geochemistry of the Assemion and Khaje-Jamali chromitite deposits in the Neyriz ophiolite were reported by Rajabzadeh et al., (1998). In addition, Jannessary et al. (2012) studied the major element and PGE geochemistry, as well as the Os-isotopic composition of chromitite deposits in southern and southeastern Iran (Neyriz, Sikhvoran, Abdasht, and Fariab) (Fig. 1a). More than 70 chromite deposits and prospects have been discovered in Iran; Sabzevar, Hormozgan, (Faryab and Esfandagheh), Neyriz (Cheshmeh-Bid) and Makran are the most important of them (Yaghubpur 2005, Jannessary et al 2012).

The Cheshmeh-Bid chromite ore deposit, hosted by the Neyriz ophiolite, is located 100 km northwest of Neyriz city. On the basis of the Cheshmeh-Bid mine report, this deposit is the biggest active mine in the Neyriz complex with a grade of 52%−53% and tonnage 0.2 ma (Taghipour et al., 2015). This study focuses on the mineralogy, textural relationships and geochemistry of trace (Ti, Mn, Ga, V, Zn, Co, Ni, and Sc) and platinum-group elements of the Cheshmeh-Bid chromitite deposit in order to determine the parent magma affinity, partial melting processes of the host rocks, and their tectonic setting. In addition, a comparison with other Iranian podiform chromitites and host peridotites is made to check the petrological and geochemical similarity and/ or differences between them.

2 Geological Setting

Late Cretaceous ophiolites in the Mediterranean eastward through Turkey, Syria, Iran, Oman, Afghanistan, and into Pakistan are fossil slices of the Neo-Tethyan oceanic lithosphere (Robertson, 2002, Shafaii Moghadam et al., 2010). Zagros ophiolites from Cyprus to Oman constitute a tract of oceanic lithosphere that formed along the southern margin of Eurasia during a subduction initiation event (Shafaii Moghadam et al., 2010). Because of similarity in ages and supra-subduction zone chemistry, these ophiolites termed the Mediterranean-Oman ophiolite belt (Mukasa and Ludden, 1987). Ophiolite-associated chromitites in Iran are related to spreading and closing of the Paleothetys in the northeast of the Neothetys in the west and southwest of Iran (Stocklin, 1974, e.g. Berberian and King, 1981; Alavi, 1994). Middle to Late Paleozoic

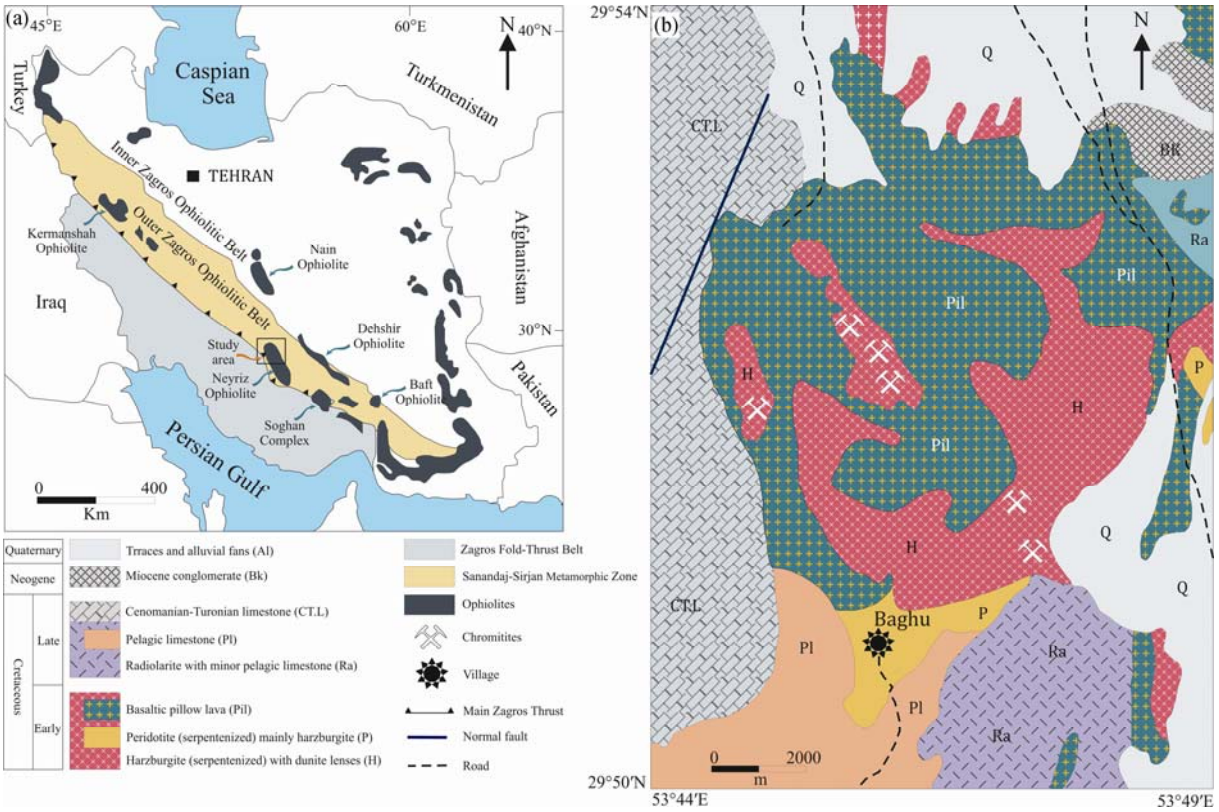

Fig. 1. Simplified tectonic map of Iran showing the distribution of the Neotethyan ophiolites and Zagros suture zones (modified from Rajabzadeh, 1998; Jaavid, 2012; Shafaii Moghadam et al., 2014; Najafzadeh and Ahmadipour, 2016).
(a), Map showing the location of the study area and the distribution of the inner and outer Zagros ophiolitic belts; (b), Simplified geological map of the study area.

ophiolites, remnants of the Paleotethys, occur aligned in northern Iran: the Aghdarband, Mashhad and Rasht ophiolites (Shafaii Moghadam et al., 2009). Other Iranian ophiolites such as the central Iranian ophiolite belt and ophiolites in Neyriz, Sabzevar, Kermanshah, Oman and northern Iraq are related to the Neothetys closure. They are residual parts of the Neothetys oceanic crust which were thrust onto the southeastern part of the Sanandaj-Sirjan metamorphic zone along the main Zagros thrust (outer part of the Neothetys ophiolite belt) after the Cretaceous, or around the Central Iranian Microcontinent (inner belt), thus forming the Dehshir-Baft, Esfandagheh and Fariab ophiolite mélange (Stocklin, 1974; Ricou, 1971; Jannessary et al., 2012) (Fig. 1a).

The NW-SE trending ophiolites between the Neyriz and Arsanjan extends about 120 km is the residual part of the Neotethys oceanic crust, remnants of which extend from the Taurus Mts. (Turkey) into Oman (Stocklin, 1974; Alavi, 1994). Ophiolites occur as scattered exposures and as individual bodies surrounded by the Quaternary formations along the main Zagros thrust fault (Fig. 1a). The Neyriz ophiolite is composed of three imbricated sheets that included: the Pichukan series, the ophiolitic unit and mélange units (Ricou, 1976; Ricou et al., 1977). The Pichakun series consists of a sequence of the Late Triassic limestones, middle Jurassic oolitic limestones, and lower-middle Cretaceous conglomeratic limestones, representing Neotethys marine sediments and unconformably overlain by Late Cretaceous Tarbur Formation (Ricou, 1976; Babaie et al., 2000; Shafaii Moghadam et al., 2014). The sequence of the Neyriz ophiolite is composed of mylonitic harzburgite and lherzolite, pegmatite gabbros, residual dunite, pyroxenite to wehrlite sills/dikes, podiform chromitite, doleritic basaltic dikes and leucogabbro lenses (Fig. 2). Harzburgites and lherzolites are characterized by high-temperature foliation, signified by alignment of stretched orthopyroxene and spinel grains. Dunites occur as variably sized discordant lenses and dikes within harzburgites. Podiform chromitites (massive or nodular) are found within depleted harzburgites, typically enveloped by dunite bodies of varying size (Shafaii Moghadam et al., 2014). The top of the mantle sequence is characterized by highly impregnated peridotites with olivine-bearing melanogabbro, layered leucogabbro, and pyroxenite cumulate sills and lenses. Gabbros are found generally as lenses within mantle peridotites. They vary from olivine-bearing melanogabbros to plagioclase-rich leucogabbros (Shafaii Moghadam and Stern, 2011a; Shafaii Moghadam et al., 2014). In addition, the Neyriz ophiolite crustal

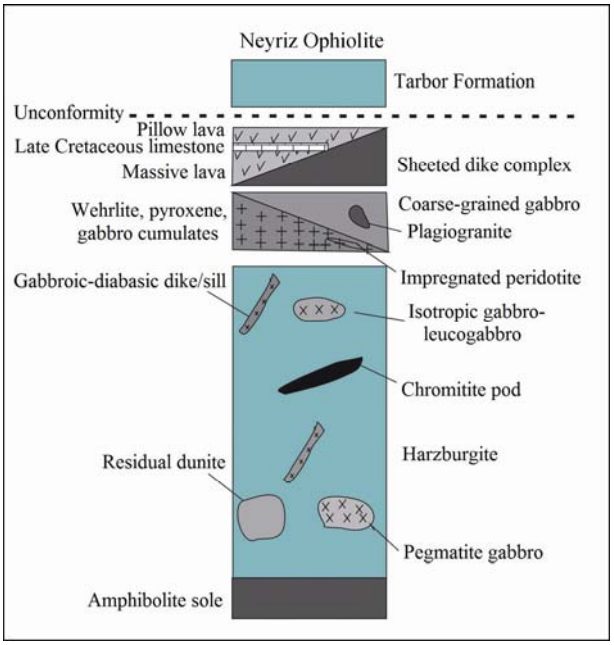

Fig. 2. Simplified stratigraphic columns displaying idealized internal lithologic successions of the Neyriz ophiolite. (modified from Shafaii Moghadam et al., 2014).

sequence consists of highly fragmented sheeted dikes and pillowed to massive basalts, accompanied by cherty and late Cretaceous pelagic limestones (Fig. 2) (Shafaii Moghadam et al., 2014). The sheeted dike complex comprises both felsic (dacitic to andesitic) dikes and mafic (diabasic) dikes, and the abundance of felsic dikes is noteworthy. Pillow lavas are highly fragmented but their contact with pelagic sediments is sometimes preserved. Pelagic sediments contain Cenomanian-Turonian to early Santonian microfaunas (Rajabzadeh et al., 2013). The mélange unit located approximately 2.5–5 km ENE of the Neyriz ophiolite includes a high-grade metamorphic mélange at the bottom and an upper sedimentary mélange at the top (Sarkarinejad, 2003). $^{40}Ar/^{39}Ar$ dating of the Neyriz ophiolites yielded 98−96 Ma ages for hornblende from plagiogranite (Haynes and Reynold, 1980). These ophiolites are unconformably overlain by the late Cretaceous Tarbur formation. Therefore possible emplacement age of the Neyriz ophiolites is late Cretaceous (Ricou, 1977).

In the Neyriz complex, several occurrences of podiform chromitite were reported by Jannessary et al., (2012), including Khajeh Jamali, Cheshmeh-Bid, and Tang-e-Hana. The Khajeh Jamali chromitite mine occurs in harzburgite and dunite with chromite potential of 0.2 million (Rajabzadeh, 1998). The massive and nodular chromitite of the Cheshmeh-Bid deposit enveloped by harzburgite and dunite haoles (Taghipour et al., 2015). The Cheshmeh-Bid chromitite characterized by medium to coarse gain, and cataclastic massive ore. The Tang-e-Hana small chromitite lens occurs in the serpentinized harzburgite (Jannessary et al., 2012). Most of the Neyriz podiform chromitite are suboriented to the foliation of the peridotite host rock. They are concordant to subconcordant relative to the host rock.

An ophiolitic complete sequence is not exposed in the Cheshmeh-Bid region. The chromitite hosting ultramafic bodies in the Cheshmeh-Bid area is relatively small, northwest trending, lens-shaped, isolated blocks composed of serpentinized harzburgite and dunite rocks (Fig. 1b). Harzburgites are the most abundant rock exposed within the complex. Serpentinized dunite and coarse-grained cumulate pyroxenite occur as small lenses. Radiolarites are present in the southeastern part of the Cheshmeh-Bid ultramafic rocks and associated with pelagic ocean floor limestones. These radiolarites are upper Jurassic-lower Cretaceous in age (Babaie et al., 2000). Dolerite dikes, single or forming swarms, have thicknesses of 3 to 4 m and cut the ultramafic rocks. The western part of the region is made up of Albian-Cenomanian Sarvak Formation limestones; these are overthrust by ophiolites (Fig. 3a). The dunite halos are surrounded by brecciated harzburgites and occur as small pods to elongated lenses and relatively extended deformational layers and range in extension from a few m to a few km (Fig. 3b). The contacts between dunites and harzburgites are sharp, but the original structural geometry of the dunites and harzburgites has been obliterated by extensive faulting and deformation.

The chromitite rocks occur mainly as small lenticular bodies, layers, and pods within serpentinized rocks of the Neyriz ophiolite. In all of the types of chromitite ore bodies (nodular or massive) the contacts between the ores and the host peridotites are commonly sharp (Fig. 3c and d). Nodular chromitite ores comprise rounded matrix-supported chromite nodules in a serpentinized dunite host. The sizes of nodules vary from 0.3 to 4 cm in diameter (Fig. 3e). The boundaries between chromitite and dunites are generally well defined (Fig. 3c). In the Cheshmeh-Bid chromitite, the tabular or layer shapes with 0.5–8 m in thickness and 35–50 m in wide are developed parallel to the peridotite banding and their lateral extent reaches up to 450 m. In these ore bodies, chromitite vary from disseminated into massive and show fine-grained disseminations of chromian spinel through to coarse-grained nodular to massive coarse-grained nodular chromitite ores.

3 Methodology

Representative samples of harzburgite and dunite envelopes, and chromitites collected during field work for

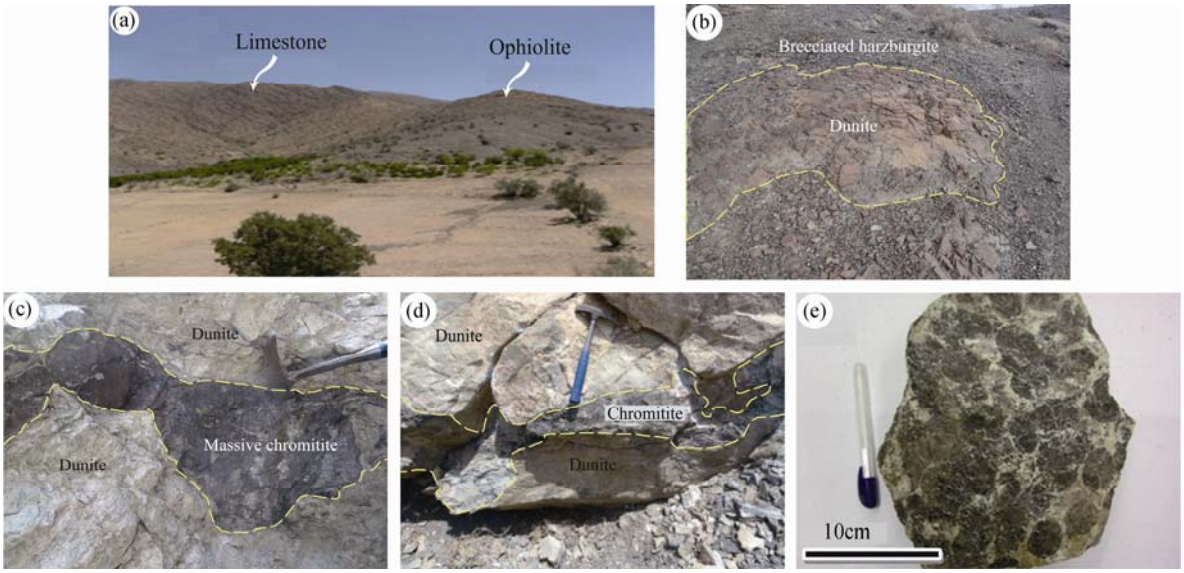

Fig. 3. Field photographs of the chromitites and associated ultramafic rocks from the Cheshmeh-Bid.
(a), Ophiolite thrust onto the Sarvak formation limestone; (b), General view of the Neyriz peridotite; Dunite serpentinized hills occurs as cream color; (c), Podiform massive chromitite which cross cut serpentinite host rock; (d), Chromitite sample of the Cheshmeh-Bid orebody; (e), Nodular chromite in a serpentinized groundmass.

mineralogical and geochemical investigations. Seventy polished and thin sections studied by reflected and transmitted microscopy at the Shiraz University. Twenty polished sections were examined chromian spinel in the chromitite, dunite, and harzburgite using a CAMECA SX50 electron microprobe at the Iranian Mineral Processing Research Center (IMIDRO). The applied accelerating voltage was 20 kV, and specimen current was 20 nA. Analytical errors are <0.5 wt% and <0.1 wt% for major and minor oxides respectively. Quantitative (WDS) microprobe analyses carried out using the crystals TAP (Si, Al), PET (Ti, Ca, and K), RAP and LiF (Fe, Na). All quantitative major element analyses were calibrated the following: Fe: Fe_2O_3; Si: wollastonite; Mg: MgO, K: orthoclase; Ca, Al: anorthite; Ti: $MnTiO_3$; Na: albite. The calculation of Fe^{2+} and Fe^{3+} in chromitite samples was done using Droop's equation ($F = 2\times(1-T/S)$ (Droop, 1987). The $Mg^{\#}$, $Cr^{\#}$ and $Fe^{3+\#}$ were calculated from atomic ratios using $Mg/(Mg+Fe^{2+})$, $Cr/(Cr+Al)$ and $Fe^{3+}/(Fe^{3+}+Cr+Al)$ formula, respectively (Tables 1–3).

A total of 16 representative samples of chromitites and associated dunites and harzburgites of the Cheshmeh-Bid deposit were selected and analyzed for all PGE (Os, Ir, Ru, Rh, Pt, and Pd). The very low PGE contents impose the use of a combined procedure of pre-concentration and matrix elimination prior to the detection with ICP-MS. This was achieved by fire assay with nickel sulfide collection (mixing the sample with a mixture of soda ash, borax, silica sulfur and nickel carbonate or nickel oxide). Samples up to 50 g in size are fire assayed using a Ni-sulfide fire assay procedure. After pre concentration, the sample solution was analyzed using Perkin-Elmer Sciex ELAN 9000 ICPMS at the Genalysis Laboratory Services Pty. Ltd. at Maddington, Western Australia. Corrections are made, where applicable, for isobaric isotopic interferences and polyatomic interferences. Laboratory standards were used for instrument calibration and drift correction. Analytical accuracy and precision were checked using standards; AMIS0076, AMIS0124, HGMN1 and by analyzing blanks and duplicates. Based on reference samples analyzed during several years in the lab recovery was estimated to be better than 85%, which is in the range of the efficiency usually obtained by Ni-sulfide fire assay. Detection limits are 2 ppb for Os, Ir, Ru, Pt and Pd and 1 ppb for Ru (Table 4). Sixteen samples of the massive Cheshmeh-Bid chromitite deposit, dunite and harzburgite envelope were analyzed for determining trace element contents. Inductively-coupled plasma mass-spectrometry (ICP-MS) analyses were carried out at ACME laboratories, Canada. Chromitite and dunite trace element content determined by ICP-Mass spectrometry following a Lithium metaborate/tetraborate fusion and nitric acid digestion of a 0.2 g sample. In addition, a separate 0.5 g split is digested in Aqua Regia and analyzed by ICP- Mass Spectrometry to report trace elements. The detection limits for trace elements vary from 0.1 ppm to 20 ppm (Table 5).

4 Petrography

4.1 Chromitite

Chromitite pods have an alignment with tabular and lenticular shapes of various sizes and have been classified into concordant to subconcordant chromitite types of

Table 1 Representative electron microprobe analyses of chromian spinel in chromitite of the Cheshmeh-Bid deposit

Lithology	Chromitite												
Sample No.	Ch-C-1	Ch-C-2	Ch-C-3	Ch-C-4	Ch-C-5	Ch-C-6	Ch-C-7	Ch-C-8	Ch-C-9	Ch-C-10	Ch-C-11	Ch-C-12	Ch-C-13
Major oxides, weight percent (wt%)													
SiO_2	0.00	0.00	0.00	0.04	0.09	0.00	0.05	0.00	0.00	0.00	0.00	0.11	0.00
TiO_2	0.20	0.18	0.16	0.12	0.19	0.14	0.22	0.16	0.16	0.19	0.18	0.17	0.14
Al_2O_3	13.26	12.41	12.05	11.26	13.79	11.85	14.61	12.01	12.41	13.36	12.73	12.91	11.21
Cr_2O_3	57.19	58.77	60.23	60.86	56.21	60.47	56.54	59.73	59.22	57.84	58.65	58.06	59.92
Fe_2O_3	1.78	1.89	1.94	1.39	2.36	0.60	1.34	1.39	1.06	1.88	0.96	1.92	1.22
FeO	12.36	13.81	12.83	13.62	14.29	14.80	12.06	12.69	13.24	14.09	13.53	13.42	14.13
MnO	0.17	0.00	0.09	0.11	0.00	0.00	0.13	0.00	0.00	0.00	0.10	0.08	0.05
MgO	13.93	12.76	12.46	12.08	12.63	12.05	14.47	13.91	13.79	12.58	13.49	13.02	13.15
CaO	0.03	bdl	bdl	0.03	bdl	bdl	bdl	bdl	0.01	bdl	0.03	0.02	bdl
NiO	0.13	0.09	0.11	0.12	0.09	0.10	0.08	0.09	0.07	0.10	0.06	0.05	0.08
Total	99.04	99.91	99.87	99.63	99.65	100.01	99.50	99.98	99.96	100.04	99.73	99.76	99.90
Number of ions based on 4 oxygen atoms													
Si	0.000	0.000	0.000	0.001	0.003	0.000	0.002	0.000	0.000	0.000	0.000	0.004	0.000
Ti	0.005	0.004	0.004	0.003	0.005	0.003	0.005	0.004	0.004	0.005	0.004	0.004	0.003
Al	0.500	0.469	0.456	0.430	0.520	0.451	0.544	0.452	0.467	0.503	0.480	0.487	0.426
Cr	1.448	1.491	1.529	1.559	1.422	1.543	1.412	1.508	1.495	1.461	1.484	1.468	1.529
Fe^{+3}	0.043	0.046	0.047	0.034	0.057	0.015	0.032	0.033	0.025	0.045	0.023	0.046	0.030
Fe^{+2}	0.331	0.370	0.344	0.369	0.382	0.399	0.318	0.339	0.353	0.376	0.362	0.359	0.381
Mn	0.005	0.000	0.002	0.003	0.000	0.000	0.003	0.000	0.000	0.000	0.003	0.002	0.001
Mg	0.665	0.610	0.596	0.583	0.602	0.579	0.681	0.662	0.656	0.599	0.643	0.621	0.632
Ca	0.001	bdl	bdl	0.001	bdl	bdl	bdl	bdl	0.000	bdl	0.001	0.001	bdl
Ni	0.003	0.002	0.003	0.003	0.002	0.003	0.002	0.002	0.002	0.002	0.002	0.001	0.002
Total	3.000	2.993	2.981	2.986	2.993	2.993	2.999	3.000	3.002	2.991	3.003	2.993	3.004
Cr#	0.743	0.761	0.770	0.784	0.732	0.774	0.722	0.769	0.762	0.744	0.756	0.751	0.782
$Mg^{\#}$	0.668	0.622	0.634	0.613	0.612	0.592	0.681	0.661	0.650	0.614	0.640	0.634	0.624
$Fe^{\#}$	0.332	0.378	0.366	0.387	0.388	0.408	0.319	0.339	0.350	0.386	0.360	0.366	0.376
$Fe^{3+\#}$	0.022	0.023	0.023	0.017	0.028	0.007	0.016	0.017	0.013	0.022	0.012	0.023	0.015
Al_2O_3 melt	12.435	12.091	11.938	11.584	12.642	11.850	12.943	11.920	12.091	12.476	12.224	12.297	11.561
TiO_2 melt	0.309	0.285	0.259	0.207	0.297	0.234	0.333	0.259	0.259	0.297	0.285	0.272	0.234
(FeO/MgO) melt	0.716	0.856	0.806	0.875	0.917	0.971	0.691	0.719	0.765	0.902	0.806	0.823	0.837
Lithology	Chromitite												
Sample No.	Ch-C-14	Ch-C-15	Ch-C-16	Ch-C-17	Ch-C-18	Ch-C-19	Ch-C-20	Ch-C-21	Ch-C-22	Ch-C-23	Ch-C-24	Ch-C-25	
Major oxides, weight percent (wt%)													
SiO_2	0.00	0.00	0.07	0.08	0.00	0.04	0.00	0.00	0.10	0.14	0.09	0.00	
TiO_2	0.14	0.19	0.22	0.13	0.21	0.14	0.17	0.19	0.15	0.13	0.12	0.18	
Al_2O_3	13.90	12.70	12.34	11.15	13.90	13.07	13.40	13.50	12.60	11.90	12.70	14.20	
Cr_2O_3	58.40	59.87	57.30	59.84	56.50	56.80	57.26	57.60	57.10	58.40	56.20	55.60	
Fe_2O_3	0.62	1.48	2.41	1.62	1.83	2.05	1.95	1.78	2.13	1.82	1.65	1.44	
FeO	12.66	13.57	12.58	12.85	12.91	13.53	13.60	12.87	12.15	13.74	13.88	13.95	
MnO	0.00	0.00	0.15	0.11	0.06	0.14	0.00	0.00	0.12	0.10	0.19	0.08	
MgO	14.03	12.11	14.25	13.51	14.10	13.60	13.55	14.00	14.88	13.20	13.96	14.11	
CaO	0.03	0.01	bdl	0.03	bdl	bdl	bdl	bdl	0.02	0.02	bdl	0.03	
NiO	0.09	0.07	0.04	0.09	0.04	0.06	0.04	0.01	0.00	0.07	0.05	0.12	
Total	99.84	99.99	99.36	99.38	99.55	99.43	99.97	99.95	99.23	99.50	98.84	99.68	
Number of ions based on 4 oxygen atoms													
Si	0.000	0.000	0.002	0.003	0.000	0.001	0.000	0.000	0.003	0.005	0.003	0.000	
Ti	0.003	0.005	0.005	0.003	0.005	0.003	0.004	0.005	0.004	0.003	0.003	0.004	
Al	0.519	0.479	0.466	0.424	0.521	0.494	0.503	0.505	0.474	0.452	0.483	0.532	
Cr	1.462	1.517	1.451	1.527	1.420	1.439	1.441	1.445	1.442	1.488	1.434	1.398	
Fe^{+3}	0.015	0.036	0.058	0.039	0.044	0.049	0.047	0.042	0.051	0.044	0.040	0.034	
Fe^{+2}	0.335	0.363	0.337	0.347	0.343	0.363	0.362	0.341	0.324	0.370	0.375	0.371	
Mn	0.000	0.000	0.004	0.003	0.002	0.004	0.000	0.000	0.003	0.003	0.005	0.002	
Mg	0.662	0.578	0.680	0.650	0.668	0.649	0.643	0.662	0.708	0.634	0.671	0.669	
Ca	0.001	0.000	bdl	0.001	bdl	bdl	bdl	bdl	0.001	0.001	bdl	0.001	
Ni	0.002	0.002	0.001	0.002	0.001	0.002	0.001	0.000	0.000	0.002	0.001	0.003	
Total	2.999	2.980	3.005	2.999	3.003	3.004	3.001	3.000	3.010	3.000	3.016	3.013	
$Cr^{\#}$	0.738	0.760	0.757	0.783	0.732	0.745	0.741	0.741	0.753	0.767	0.748	0.724	
$Mg^{\#}$	0.664	0.614	0.669	0.652	0.661	0.642	0.640	0.660	0.686	0.631	0.642	0.643	
$Fe^{\#}$	0.336	0.386	0.331	0.348	0.339	0.358	0.360	0.340	0.314	0.369	0.358	0.357	
$Fe^{3+\#}$	0.007	0.018	0.029	0.020	0.022	0.025	0.023	0.021	0.026	0.022	0.020	0.018	
Al_2O_3 melt	12.683	12.212	12.062	11.533	12.683	12.362	12.492	12.531	12.171	11.872	12.212	12.794	
TiO_2 melt	0.234	0.297	0.333	0.220	0.321	0.234	0.272	0.297	0.247	0.220	0.207	0.285	
(FeO/MgO) melt	0.741	0.891	0.697	0.737	0.747	0.799	0.810	0.743	0.650	0.818	0.799	0.816	

Note: bdl = below detection limit.

Cassard et al. (1981). Chromites grains are characterized by massive, nodular and disseminate textures (Figs. 3c–e and 4a). Secondary textures were been recorded by cataclastic and pull-apart textures (Fig. 4b). Massive chromitite made up of 90%–95% chromite varying in grain size between 1 and 5 cm. Serpentinized olivine

Table 2 Representative electron microprobe analyses of chromian spinel in dunite and harzburgite of the Cheshmeh-Bid

Lithology	Dunite											
Sample No.	Ch-D-1	Ch-D-2	Ch-D-3	Ch-D-4	Ch-D-5	Ch-D-6	Ch-D-7	Ch-D-8	Ch-D-9	Ch-D-10	Ch-D-11	Ch-D-12
Major oxides, weight percent (wt%)												
SiO_2	0.06	0.16	0.10	0.00	0.24	0.04	0.08	0.00	0.09	0.02	0.11	0.04
TiO_2	0.07	0.11	0.09	0.13	0.08	0.10	0.08	0.05	0.06	0.07	0.11	0.05
Al_2O_3	9.98	12.80	10.44	10.27	10.86	11.75	11.28	9.62	10.93	11.32	11.69	10.27
Cr_2O_3	56.04	54.05	55.58	56.51	55.71	53.44	54.22	57.37	55.16	54.89	54.30	57.05
Fe_2O_3	3.80	2.85	3.64	2.73	3.02	3.11	4.09	3.37	4.26	3.58	2.46	2.96
FeO	19.86	18.55	19.26	19.72	19.44	20.43	20.61	19.60	18.79	18.04	20.59	19.83
MnO	0.20	0.18	0.31	0.13	0.10	0.19	0.26	0.10	0.34	0.25	0.38	0.21
MgO	9.12	10.33	9.66	8.42	10.07	10.20	9.15	9.47	9.04	10.92	9.28	9.21
CaO	bdl	bdl	bdl	0.04	bdl	0.03	0.03	bdl	bdl	bdl	bdl	bdl
NiO	0.03	0.04	0.15	0.10	0.00	0.10	0.06	0.07	0.00	0.07	0.16	0.00
Total	99.16	99.07	99.23	98.05	99.52	99.39	99.86	99.65	98.67	99.16	99.08	99.62
Number of ions based on 4 oxygen atoms												
Si	0.002	0.005	0.003	0.000	0.008	0.001	0.003	0.000	0.003	0.001	0.004	0.001
Ti	0.002	0.003	0.002	0.003	0.002	0.002	0.002	0.001	0.002	0.002	0.003	0.001
Al	0.395	0.496	0.411	0.411	0.424	0.460	0.442	0.379	0.432	0.441	0.460	0.404
Cr	1.489	1.407	1.469	1.519	1.461	1.404	1.426	1.518	1.463	1.436	1.435	1.506
Fe^{+3}	0.096	0.071	0.092	0.070	0.075	0.078	0.102	0.085	0.107	0.089	0.062	0.074
Fe^{+2}	0.558	0.510	0.538	0.560	0.539	0.567	0.573	0.548	0.527	0.499	0.575	0.554
Mn	0.006	0.005	0.009	0.004	0.003	0.005	0.007	0.003	0.010	0.007	0.011	0.006
Mg	0.457	0.507	0.481	0.427	0.498	0.505	0.453	0.472	0.452	0.538	0.462	0.458
Ca	bdl	bdl	bdl	0.001	bdl	0.001	0.001	bdl	bdl	bdl	bdl	bdl
Ni	0.001	0.001	0.004	0.003	0.000	0.003	0.002	0.002	0.000	0.002	0.004	0.000
Total	3.006	3.005	3.009	2.998	3.010	3.027	3.011	3.008	2.995	3.015	3.015	3.005
$Cr^{\#}$	0.790	0.739	0.781	0.787	0.775	0.753	0.763	0.800	0.772	0.765	0.757	0.788
$Mg^{\#}$	0.450	0.498	0.472	0.432	0.480	0.471	0.442	0.463	0.462	0.519	0.445	0.453
$Fe^{\#}$	0.550	0.502	0.528	0.568	0.520	0.529	0.558	0.537	0.538	0.481	0.555	0.547
$Fe^{3+\#}$	0.049	0.036	0.046	0.035	0.038	0.040	0.052	0.043	0.054	0.045	0.032	0.037
Lithology	Dunite		Harzburgite									
Sample No.	Ch-D-13	Ch-D-14	Ch-H-1	Ch-H-2	Ch-H-3	Ch-H-4	Ch-H-5	Ch-H-6	Ch-H-7	Ch-H-8	Ch-H-9	Ch-H-10
Major oxides, weight percent (wt%)												
SiO_2	0.01	0.00	0.00	0.06	0.10	0.00	0.03	0.07	0.07	0.05	0.00	0.02
TiO_2	0.06	0.07	0.04	0.03	0.04	0.06	0.05	0.02	0.02	0.07	0.03	0.05
Al_2O_3	11.81	10.70	22.37	18.24	20.62	23.71	19.35	20.49	19.07	23.38	21.52	21.30
Cr_2O_3	53.28	55.33	47.12	50.77	48.56	45.28	47.73	48.11	50.58	46.16	46.45	45.89
Fe_2O_3	2.62	2.90	1.32	1.55	1.10	1.41	2.48	1.24	1.92	1.63	2.23	2.61
FeO	19.35	19.58	17.06	17.71	16.13	16.10	17.43	17.15	16.26	15.14	16.30	18.55
MnO	0.17	0.15	0.17	0.16	0.12	0.18	0.16	0.04	0.19	0.22	0.10	0.15
MgO	10.56	10.15	11.81	11.25	13.37	13.06	11.62	12.68	11.76	13.25	12.53	10.49
CaO	0.01	0.01	bdl	0.04	bdl	0.02	0.03	bdl	0.02	0.04	bdl	0.01
NiO	0.15	0.22	0.03	0.13	0.04	0.09	0.06	0.00	0.05	0.03	0.04	0.18
Total	98.02	99.11	99.92	99.94	100.08	99.91	98.94	99.80	99.94	99.97	99.20	99.25
Number of ions based on 4 oxygen atoms												
Si	0.000	0.000	0.000	0.002	0.003	0.000	0.001	0.002	0.002	0.002	0.000	0.001
Ti	0.002	0.002	0.001	0.001	0.001	0.001	0.001	0.000	0.000	0.002	0.001	0.001
Al	0.467	0.421	0.817	0.681	0.753	0.857	0.725	0.754	0.706	0.843	0.792	0.793
Cr	1.412	1.462	1.155	1.273	1.190	1.098	1.200	1.188	1.256	1.117	1.147	1.147
Fe^{+3}	0.066	0.073	0.031	0.037	0.026	0.033	0.059	0.029	0.045	0.038	0.052	0.062
Fe^{+2}	0.542	0.547	0.442	0.469	0.418	0.413	0.463	0.448	0.427	0.387	0.426	0.490
Mn	0.005	0.004	0.004	0.004	0.003	0.005	0.004	0.001	0.005	0.006	0.003	0.004
Mg	0.528	0.505	0.546	0.531	0.617	0.597	0.551	0.590	0.550	0.604	0.583	0.494
Ca	0.000	0.000	bdl	0.001	bdl	0.001	0.001	bdl	0.001	0.001	bdl	0.000
Ni	0.004	0.006	0.001	0.003	0.001	0.002	0.002	0.000	0.001	0.001	0.001	0.005
Total	3.026	3.020	2.997	3.003	3.012	3.006	3.007	3.012	2.995	2.999	3.004	2.997
$Cr^{\#}$	0.752	0.776	0.586	0.651	0.612	0.562	0.623	0.612	0.640	0.570	0.592	0.591
$Mg^{\#}$	0.493	0.480	0.552	0.531	0.596	0.591	0.543	0.569	0.563	0.609	0.578	0.502
$Fe^{\#}$	0.507	0.520	0.448	0.469	0.404	0.409	0.457	0.431	0.437	0.391	0.422	0.498
$Fe^{3+\#}$	0.034	0.037	0.015	0.019	0.013	0.016	0.030	0.015	0.023	0.019	0.026	0.031

Note: bdl = below detection limit.

(mainly antigorite), chlorite and trace amount chalcopyrite are the other associated mineral. Nodular chromitite is mostly hosted by dunite but also forms halos around massive chromitite (Fig. 3e). Elliptical chromite nodules of 0.3 to 4 cm in size occur in a groundmass of serpentinized olivine. Olivine crystals in the margins of chromitite lenses have been recrystallized to granoblasts. Dunite envelopes are composed of 95% olivine and 1%–3% disseminated chromite and orthopyroxene and texturally characterized by recrystallized olivine (Fig. 4a). Chromitites and their dunitic halos are surrounded by harzburgite.

4.2 Dunite and harzburgite

Dunite envelopes are composed of 95% olivine and 1%–3% disseminated chromite and orthopyroxene (Fig. 4c). Chromitites and their dunitic halos are surrounded by harzburgite. Harzburgites are composed of 60%–70%

Table 3 Results of EPMA analyses of olivine in the Cheshmeh-Bid peridotites

Lithology	Dunite										
Sample No.	Ch-D-1	Ch-D-2	Ch-D-3	Ch-D-4	Ch-D-6	Ch-D-7	Ch-D-8	Ch-D-9	Ch-D-10	Ch-D-12	Ch-D-14
Major oxides, weight percent (wt%)											
SiO_2	41.27	40.95	41.23	41.34	41.50	41.07	41.03	41.35	41.10	41.06	41.43
TiO_2	0.02	0.02	0.05	0.02	0.02	0.10	bdl	0.02	0.02	0.01	bdl
Al_2O_3	bdl	0.02	0.02	0.02	bdl	0.10	bdl	0.01	bdl	bdl	0.01
Cr_2O_3	bdl	bdl	bdl	0.03	bdl	bdl	0.01	bdl	0.03	0.01	0.01
FeO_t	8.16	8.08	7.81	8.31	7.85	8.28	8.01	8.11	7.87	7.63	7.92
MnO	0.04	0.10	0.13	0.12	0.07	0.06	0.11	0.10	0.00	0.14	0.07
MgO	51.48	51.43	51.16	50.86	50.45	50.84	52.42	50.69	51.47	51.77	50.65
CaO	0.04	0.29	bdl	0.03	0.05	0.08	0.02	0.02	0.10	0.07	bdl
NiO	0.35	0.05	0.40	0.19	0.36	0.30	0.33	0.39	0.28	0.30	0.32
Total	101.42	100.94	100.80	100.92	100.30	100.83	101.93	100.69	100.87	100.99	100.41
Number of ions based on 4 oxygen atoms											
Si	0.991	0.990	0.995	0.997	1.005	0.993	0.981	0.999	0.992	0.989	1.002
Ti	0.000	0.000	0.001	0.000	0.000	0.002	0.000	0.000	0.000	0.000	0.000
Al	0.000	0.001	0.001	0.001	0.000	0.003	0.000	0.000	0.000	0.000	0.000
Cr	0.001	0.000	0.000	0.001	0.000	0.000	0.000	0.000	0.001	0.000	0.000
Fe^{+2}	0.164	0.163	0.158	0.168	0.159	0.167	0.160	0.164	0.159	0.154	0.160
Mn	0.001	0.002	0.003	0.002	0.001	0.001	0.002	0.002	0.000	0.003	0.001
Mg	1.843	1.853	1.840	1.829	1.822	1.832	1.869	1.826	1.851	1.859	1.827
Ca	0.001	0.008	bdl	0.001	0.001	0.002	0.001	0.001	0.003	0.002	bdl
Ni	0.007	0.001	0.008	0.004	0.007	0.006	0.006	0.008	0.005	0.006	0.006
Total	3.009	3.017	3.004	3.003	2.996	3.006	3.019	3.001	3.010	3.013	2.997
Fo	91.80	91.81	91.99	91.49	91.91	91.57	92.00	91.67	92.10	92.23	91.87
Fa	8.16	8.09	7.88	8.38	8.02	8.37	7.89	8.23	7.90	7.62	8.06

Lithology	Harzburgite								
Sample No.	Ch-H-1	Ch-H-3	Ch-H-4	Ch-H-5	Ch-H-6	Ch-H-7	Ch-H-8	Ch-H-9	Ch-H-10
Major oxides, weight percent (wt%)									
SiO_2	41.77	42.20	41.18	41.47	40.74	41.33	42.11	41.34	41.10
TiO_2	0.02	0.04	0.03	0.01	0.10	bdl	bdl	bdl	0.02
Al_2O_3	bdl	0.01	0.02	0.02	bdl	0.02	bdl	0.02	0.02
Cr_2O_3	0.01	0.02	0.05	0.04	bdl	0.02	bdl	0.01	bdl
FeO_t	8.82	8.22	8.60	8.61	8.42	8.27	8.35	8.38	8.51
MnO	0.10	0.05	0.14	0.17	0.08	0.10	0.15	0.15	0.09
MgO	50.37	50.14	50.26	50.29	49.95	50.10	50.67	50.83	49.72
CaO	0.01	bdl	bdl	0.01	0.05	bdl	0.08	bdl	0.01
NiO	0.34	0.26	0.40	0.30	0.38	0.39	0.43	0.47	0.45
Total	101.44	100.94	100.68	100.92	99.72	100.23	101.79	101.20	99.92
Number of ions based on 4 oxygen atoms									
Si	1.004	1.015	0.998	1.002	0.997	1.004	1.007	0.996	1.003
Ti	0.000	0.001	0.001	0.000	0.002	0.000	0.000	0.000	0.000
Al	0.000	0.000	0.001	0.001	0.000	0.001	0.000	0.001	0.001
Cr	0.000	0.000	0.001	0.001	0.000	0.000	0.000	0.000	0.000
Fe^{+2}	0.177	0.165	0.174	0.174	0.172	0.168	0.167	0.169	0.174
Mn	0.002	0.001	0.003	0.003	0.002	0.002	0.003	0.003	0.002
Mg	1.805	1.797	1.816	1.811	1.822	1.814	1.807	1.826	1.809
Ca	0.000	0.000	0.000	0.000	0.001	bdl	0.002	bdl	0.000
Ni	0.007	0.005	0.008	0.006	0.007	0.008	0.008	0.009	0.009
Total	2.996	2.984	3.001	2.998	3.003	2.996	2.995	3.004	2.997
Fo	90.96	91.53	91.11	91.08	91.29	91.43	91.40	91.39	91.16
Fa	8.93	8.42	8.74	8.75	8.63	8.47	8.44	8.45	8.75

Note: bdl = below detection limit.

olivine, 15%–30% orthopyroxene and smaller amounts of chromite and clinopyroxene (Fig. 4d). Orthopyroxene is 5 to 7 mm in diameter and contains exsolution lamellae of clinopyroxene (Fig. 4d). Chromite in these rocks occurs as sub- to euhedral grains dispersed in an olivine groundmass, or as inclusions in olivine and orthopyroxene (Fig. 4c and e). Locally, dispersed chromite grains may partly accumulate resulting in a disseminated texture. It suggests that magma crystallization began with olivine before chromite settling. Orthopyroxene in the matrix of serpentinized peridotite has kink bands and rounded grain margins (Fig. 4f). Orthopyroxene with rounded margins may indicate reaction between melt and peridotite (Kelemen et al., 1990). Serpentinization is common in the Cheshmeh-Bid peridotite rocks (Fig. 4g.) Chalcopyrite exists in the chromite as interstitial (Fig. 4h).

5 Geochemistry of the Chromitites and Associated Rocks

5.1 Mineral chemistry

5.1.1 Chromian spinel

Chromain spinel occurs as a relict in the dunite and harzburgite and as primary grains in chromitites. The

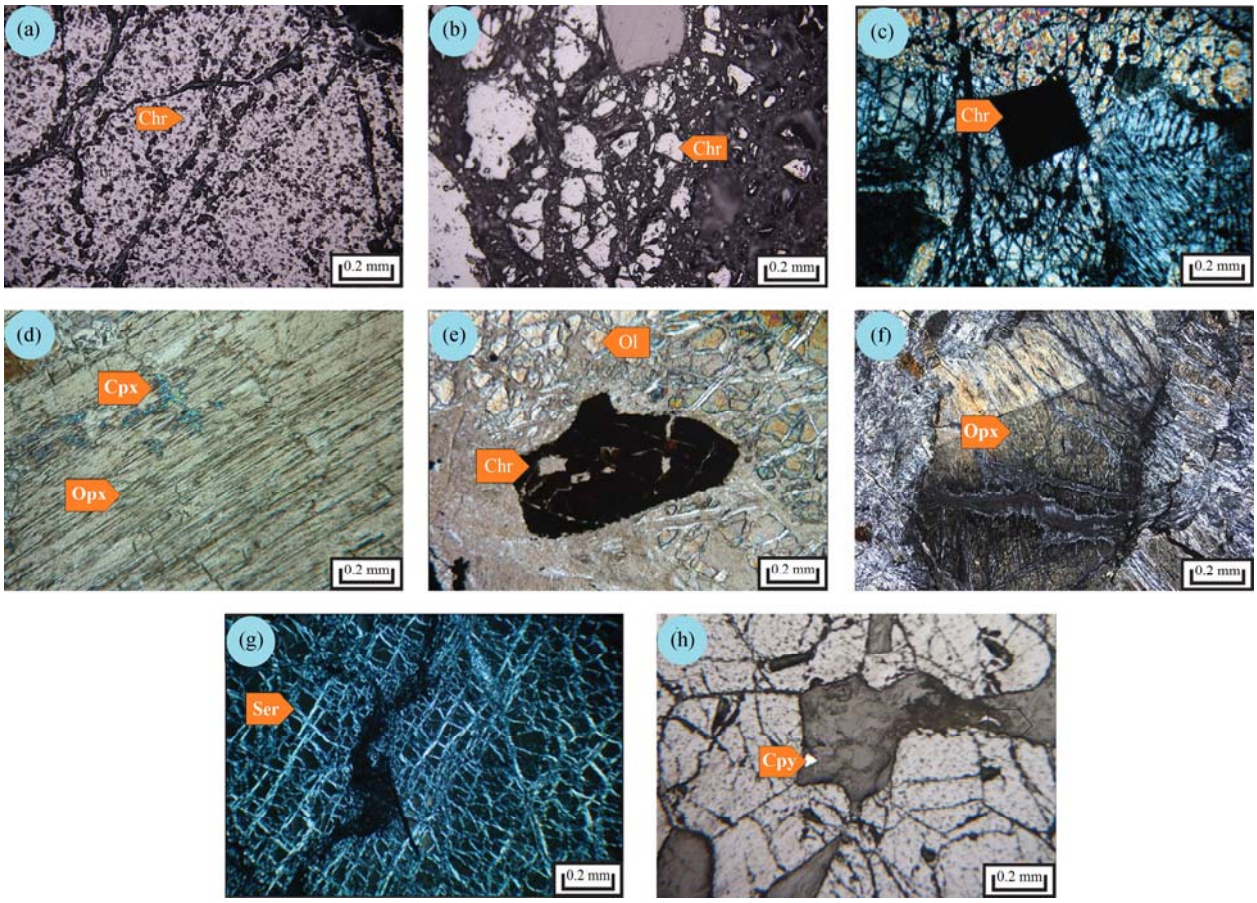

Fig. 4. Microphotographs of the chromitites and associated ultramafic rocks from the Cheshmeh-Bid.
(a), Massive texture of the Cheshmeh-Bid chromitite (ppl); (b), Cataclastic texture of the Cheshmeh-Bid chromitite (ppl); (c), Dunite envelope with brecciate texture comprised of olivine, pyroxene and euhedral chromian spinel (xpl); (d), A large crystal of orthopyroxene with exsolution lamellae of clinopyroxene in the harzburgite rock (ppl); (e), Subhedral chromian spinel in the serpentinized dunite rock, olivine grain is shown with resorbed margin (xpl); (f), Orthopyroxene in the matrix of serpentinized peridotite has kink bands and rounded grain margins (xpl); (g), serpentinized peridotite with stockwork texture as the chromitite host rock (xpl); (h), Fine-grained chalcopyrite (yellow) associated with chromite (ppl).
Chr − chromitite; Opx − orthopyroxene; Cpx − Clinopyroxene; Ol − olivine; Ser − serpentinized peridotite; Cpy − chalcopyrite.

chemical compositions of the Cheshmeh-Bid chromian spinel in chromitite, dunite and harzburgite have been shown in Tables 1 and 2. The Cr_2O_3 content varies from 56.20 wt%–60.80 wt%, 53.28 wt%–55.33 wt%, and 45.8 wt%–50.77 wt%, in chromitite, dunite, and harzburgite, respectively. The $Cr^{\#}$(Cr/Cr+Al) in massive chromitite ranges 0.72–0.78 and in dunite and harzburgite varies 0.73–0.80, and 0.56–0.77, respectively. The $Cr^{\#}$ is usually higher in chromitite (0.72–0.78) and dunite (0.74–0.80) than in harzburgite (0.56–0.77). The Cheshmeh-Bid chromitite and dunite are high-Cr, whereas harzburgite is high-Al (Fig. 5a). Increasing $Cr^{\#}$ typically correlated with increasing degrees of partial melting in the host peridotite (Dick and Bullen, 1984, Xiong et al., 2017).

The TiO_2 content is generally low in the Cheshmeh-Bid deposit, TiO_2 content varies 0.12 wt%–0.2 wt%, 0.06 wt%–0.07 wt%, and 0.02 wt%–0.07 wt% in chromitite, dunite, and harzburgite, respectively. The TiO_2 content is higher in chromitite than dunite and harzburgite. $Fe^{3+\#}$(Fe^{3+}/Fe^{3+}+Cr+Al) value in chromitite and chromian spinel of dunite and harzburgite is very low <0.04.

The $Mg^{\#}$(Mg/Mg+Fe^{2+}) value varies 0.62–0.68, 0.48–0.49, and 0.50–0.60 in chromitite, dunite and harzburgite, respectively. Therefore, the $Mg^{\#}$ is higher in massive chromitite than dunite and harzburgite. Also in the Al_2O_3 versus Cr_2O_3 binary diagram of Bonavia et al (1933), the Cheshmeh-Bid samples are the podiform type, in this diagram massive chromitite and dunite chromian spinel samples plot in the high-Cr field whereas, harzburgite chromian spinel samples plot in high- Al field (Fig. 5b). The Cheshmeh-Bid massive chromitite samples have medium $Fe^{2+\#}$(Fe^{2+}/Mg+Fe^{2+}) = 0.32–0.41. The $Fe^{2+\#}$ for chromian spinel in dunite ranges 0.48–0.57 and it ranges 0.39−0.51 in harzburgite. The chromian spinel in dunite has the highest value of the $Fe^{2+\#}$ ratio.

5.1.2 Olivine chemistry

Olivine composition in the Cheshmeh-Bid harzburgite (Fo = 90.96−91.53) and dunite (Fo = 91.49–92.23) is highly forsterite with little variation (Table 3, Fig. 6). The

Table 4 Bulk-rock analyses on platinum group elements (PGE) of representative samples of chromitites, dunites, and harzburgites from the Cheshmeh-Bid area

Lithology	Chromitite							
Sample No.	Ch-C-1	Ch-C-2	Ch-C-3	Ch-C-4	Ch-C-5	Ch-C-6	Ch-C-7	Ch-C-8
Os (ppb)	58	63	42	49	51	75	66	45
Ir	33	37	26	30	32	55	47	29
Ru	114	122	95	91	105	137	119	88
Rh	11	10	7	7	10	8	13	10
Pt	8	5	2	4	4	>2	5	2
Pd	6	4	2	3	4	3	8	>2
Total PGE	230	241	174	184	206	279	258	176
IPGE	205	222	163	170	188	267	232	162
PPGE	25	19	11	14	18	12	26	14
ΣIPGE/ΣPPGE	8.20	11.68	14.82	12.14	10.44	22.25	8.92	11.57
ΣPPGE/ΣIPGE	0.12	0.09	0.07	0.08	0.10	0.04	0.11	0.09
Pd/Ir	0.18	0.11	0.08	0.10	0.13	0.05	0.17	0.07
Pt/Pt*	0.31	0.25	0.17	0.28	0.20	0.07	0.16	0.14
Ptn/Irn	0.11	0.06	0.03	0.06	0.06	0.01	0.05	0.03
Pdn/Irn	0.09	0.05	0.04	0.05	0.06	0.03	0.08	0.03
Ptn/Pdn	1.07	0.99	0.80	1.07	0.8	0.27	0.50	0.8

Lithology	Chromitite			Dunite			Harzburgite	
Sample No.	Ch-C-9	Ch-C-10	Ch-C-11	Ch-D-1	Ch-D-2	Ch-D-3	Ch-H-1	Ch-H-2
Os	55	60	59	>2	3	5	4	4
Ir	34	45	32	2	2.5	3	3	5
Ru	102	110	121	6	9	11	13	12
Rh	10	7	13	>2	2	2	2	>2
Pt	8	3	4	8	13	9	14	10
Pd	5	5	3	7	8	10	12	14
Total PGE	214	230	232	26	37.5	40	48	46.5
IPGE	191	215	212	10	14.5	19	20	21
PPGE	23	15	20	16	23	21	28	25.5
ΣIPGE/ΣPPGE	8.30	14.33	10.60	0.63	0.63	0.90	0.71	0.82
ΣPPGE/ΣIPGE	0.12	0.07	0.09	1.60	1.59	1.11	1.40	1.21
Pd/Ir	0.15	0.11	0.09	3.50	3.20	3.33	4.00	2.80
Pt/Pt*	0.36	0.16	0.20	0.97	1.04	0.64	0.91	0.70
Ptn/Irn	0.11	0.03	0.06	1.81	2.35	1.36	2.11	0.90
Pdn/Irn	0.07	0.05	0.05	1.70	1.55	1.62	1.94	1.36
Ptn/Pdn	1.28	0.48	1.07	1.07	1.52	0.84	1.09	0.67

Note: Pt/Pt*=(Pt/8.3)/√[(Rh/1.6) × (Pd/4.4)]. The Pt anomaly (Pt/Pt*), PPGEN/IPGEN, and Pd/Ir ratios calculated according to half values which were used for statistical calculations of samples with values below detection limit.

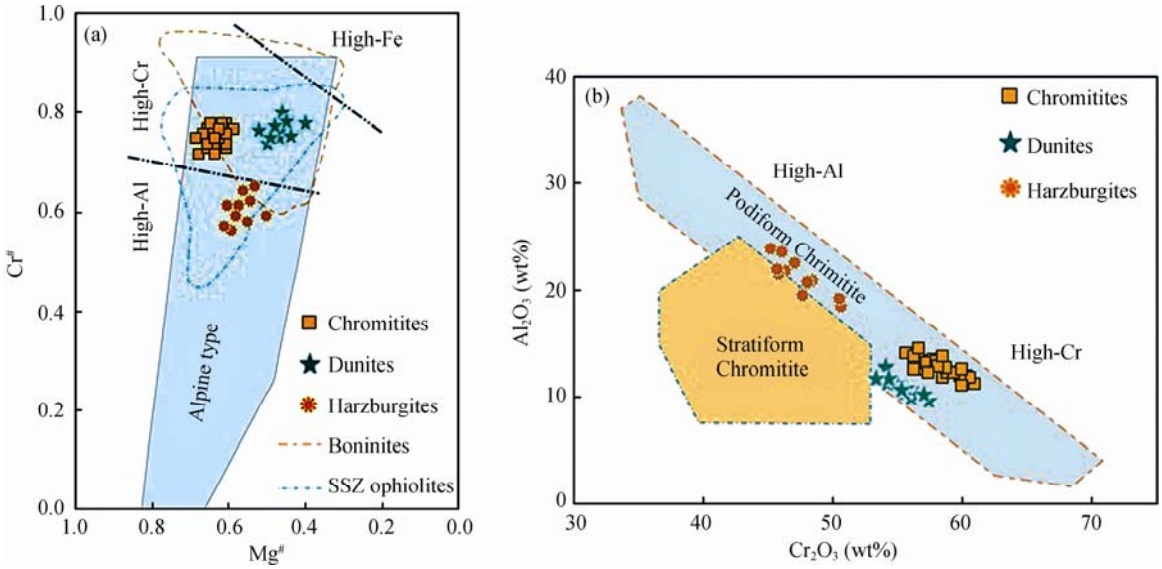

Fig. 5. Variation diagrams showing mineral compositions from the Cheshmeh-Bid chromitite.
(a), Binary diagram of the $Cr^{\#}$ versus $Mg^{\#}$ of the massive chromitie, dunite, and harzburgite chromian spinel. The Alpine-type field after Irvine (1967); Supra-subduction zone (SSZ) and boninite after Bridges et al. (1995); The high-Cr, high-Al and high- Fe chromian spinel types are from Zhou and Bai (1992); b) Chromian spinel composition from the Cheshmeh-Bid chromitite. Compositional fields of podiform and strtiform chromitite after Bonavia et al. (1993).

NiO content of olivine in the dunites ranges from 0.19 wt%–0.4 wt% (with an average of 0.32 wt%) and in harzburgites from 0.26 wt% –0.47 wt% (with an average of 0.38 wt%). The values of TiO_2, Al_2O_3, Cr_2O_3, and CaO in olivine of the Cheshmeh-Bid dunite and harzburgite are below detection limit that is very similar to the composition of the Abdasht peridotite in Iran (Najafzadeh and Ahmadipour, 2016).

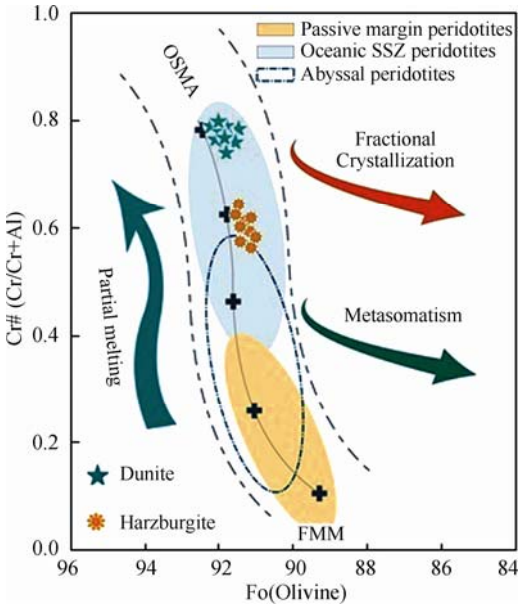

Fig. 6. Chemical variation of $Cr^{\#}$ versus Fo content of the olivine-Cr-spinel pairs in harzburgite and dunite samples.
Olivine-spinel mantle array (OSMA), melting trends and amounts of melting are from Arai (1994).

5.2 Whole-rock PGE geochemistry

Sixteen bulk samples of massive chromitite, dunite and harzburgite were analyzed for PGE (Os, Ir, Ru, Pt, and Pd) (Table 4). Total PGE content of the Cheshmeh-Bid chromitite varies between 174 to 241 ppb with an average of 220 ppb. These values are very similar to the total PGE values (155–257 ppb, average 212 ppb) which reported by Jannessary et al. (2012). The dunite and harzburgite display low total PGE abundances, ranging between 26 to 40 ppb (average of 34.5), and 40 to 46.5 ppb, (average of 47.25), respectively. Back scatter image and electron probe micro analysis which analyzed by Jannessary et al. (2012), have shown the presence of laurite and ruthenium oxide (RuO_2) as the main PGE-bearing minerals in the Cheshmeh-Bid deposit. The Cheshmeh-Bid samples are enriched in Ir-group (IPG: Os, Ir, and Ru) and depleted in the Pt-group (PPG: Ru, Pt, and Pd) (SIPGE/SPPGE = 0.8.20–22.25) (Table 4). Upper primitive mantle (PUM) normalized PGE patterns show enrichment in Os, Ir and Ru (IPGE) and a negative slope toward the Rh, Pt, and Pd (PPGE) (Fig. 7a). Furthermore, negative Pt anomalies (average of Pt_n/Pd_n = 0.83) and low Rh, Pd and Re contents are characteristic for ophiolitic chromitites (Proenza et al., 2007, Uysal et al., 2007).

The comparison of the PGE spiderdiagram of chromitite, dunite, and harzburgite indicate chromitite samples have more IPGE content than dunite and harzburgite. Dunite and harzburgite PGE spiderdiagram show similar pattern (Fig. 7b). The Ru indicates a positive anomaly in chromitite (average of 109.45 ppb, respectively), dunite (average of 8.6 ppb) and harzburgite (average of 12.5 ppb). The average values of platinum and palladium in chromitite (4.3 and 4.09 ppb, respectively) are lower than dunite (10, 8.3 ppb, respectively) and harzburgite (12, 13 ppb, respectively). The Pd_n/Ir_n ratios as index of fractionation in dunite range 3.2–3.5 (average of 3.34), it is higher than the average value (0.12) (Shen-Su, 1982), and this ratio ranges 2.80–4 with average of 3.40 in harzburgite, which is higher than the average value (1.08) (Shen-Su, 1982). Also, the high value of Ir_n/pd_n (1.75−3) in the Abdasht harzburgite (outer Zagros ophiolitic belt) is reported by Najafzadeh and Ahmadipour (2016). Burghath et al (2002) classified ophiolitic chromitites into four

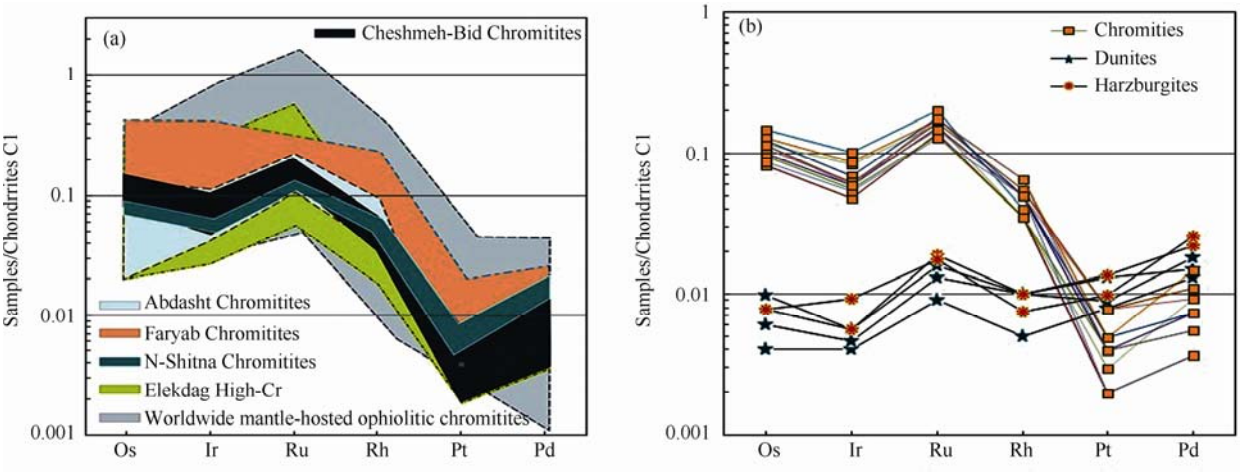

Fig. 7. Chondrite normalized PGE patterns for chromitite samples from the Cheshmeh-Bid deposit.
(a), Chondrite-normalized PGE patterns for podiform chromitites. The fields of worldwide chromitite (Economu-Eliopoulos, 1996; Garuti et al., 2005; Mcelduff and Stumpfl, 1990; Melcher et al., 1997; Proenza et., 1999; Rajabzadeh et al., 1988; Najafzadeh and Ahmadipour, 2016; Economou-Eliopoulos et al., 2017); Luobusa ultra-high pressure (UHP) (Zhou et al., 1996); N-Shitna (Ismail et al., 2014); Elekdag (Donmez et al., 2014) are used for comparison; (b), Chondrite normalized PGE for chromitite, dunite and harzburgite of the Cheshmeh-Bid chromitite. Chondrite normalized values are from Naldrett and Duck (1980).

groups based on the Pt/Ir and Pt/Pd ratios (Fig. 8a and b). Group I, termed the "normal ophiolitic type" is characterized by negative slopes in the normalized diagram from Os, to Pt and by Pt_n/Ir_n< 0.9, the total PGE content up to 7.7 ppm have been found (Fig. 8b). Group-II, the "diverging ophiolite type", is characterized by higher proportions of base metal sulfides and may carry up to 11 ppm PGE. The Pt_n/Ir_n ratio varies from 0.9 to 4.6, and the PGE pattern is commonly flat with PPGE/IPGE ~1. Group- III is dominated by Pd and abundant base metal sulfides, by Pt_n/Ir_n>1 and Pt_n/Pd_n mostly <1 (Jannessary et al., 2012). Three subgroups are distinguished based on the abundance of PGM (low in IIIa, high in IIIb) and the host rock of mineralization (chromitite in IIIa and IIIb, dunite in IIIc). Up to 23 ppm, PGE contents were recorded. Group-IV, the "Ptdominated sulfide-poor ophiolite type" is restricted to late-stage chromitites in ultramafic cumulates close to the crust-mantle transition zone (Jannessary et al., 2012). The Pt_n/Ir_n and Pt_n/Pd_n ratios are >1, and PGE contents may reach up to 25 ppm. Accordingly, most (n = 6) of the Cheshmeh-Bid chromitites investigated during this study have group-I PGE patterns characterized by Pt_n/Ir_n<0.9 and Pt_n/Pd_n<1, representing the "normal ophiolite type" .Another 5 samples have Pt_n/Pd_n>1 and are classified here as group-I* (Fig. 8a).

5.3 Whole-rock trace element geochemistry

Trace elements (Sc, Ti, V, Mn, Co, Ni, Zn, and Ga) in chromites from podiform chromitites can estimate the composition of the magma from which they have formed and explore and document the mechanism responsible for their chemical variability (Page and Barnes, 2009). Gallium and vanadium content of chromitite samples in the Cheshmeh-Bid deposit varies between 13 and 26 ppm, and 466 to 842 ppm, respectively (Table 5). These values are different from the MORB and comparable to chromitite samples of boninitic origin in northern Oman, Turkey (Dare et al., 2008) and the Thetford chromitites of Canada (i.e. high chromium chromite reported by Page and Barnes, 2009) (Fig. 9). The binary diagram of $Cr^{\#}$ versus Ga and V show a negative correlation (R = −69 and −92 respectively) (Fig. 9a and b). There is a distinctive positive correlation between gallium and vanadium (Fig.

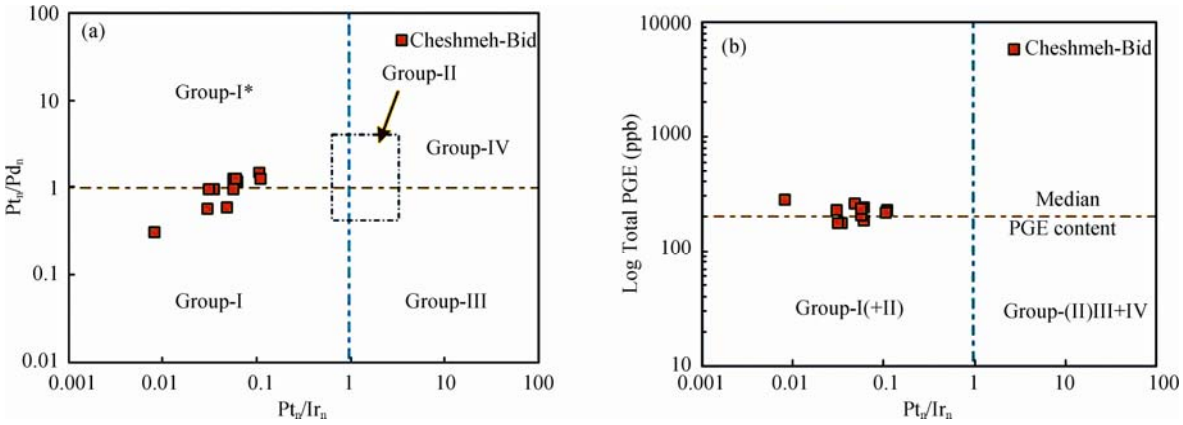

Fig. 8. (a), Mantle-normalised ratio of Pt/Ir versus Pt/Pd for chromitite, dunite, and harzburgite; (b), Normalised Pt/Ir versus total PGE content.
Group definition according to Burgath et al. (2002).

Table 5 Trace element in the Cheshmeh-Bid chromitite

Lithology		Chromitite							
Sample No.		Ch-D-2	Ch-C-3	Ch-C-5	Ch-C-7	Ch-H-8	Ch-C-11	Ch-C-12	Ch-C-14
V	*8 (ppm)	550	658	742	755	590	653	668	685
Ga	0.5	16	19	22	21	15	17	18	20
Zn	1	47	49	50	22	63	33	47	38
Ni	0.1	893	1010	1050	885	965	968	852	1210
Mn	5	1041	1007	929	1084	1054	852	1026	947
Co	0.2	167	152	142	133	160	143	162	138
Lithology		Chromitite							
Sample no.		Ch-D-16	Ch-H-17	Ch-C-18	Ch-C-20	Ch-C-22	Ch-C-23	Ch-D-24	Ch-C-25
V	*8 (ppm)	604	521	749	688	690	466	803	842
Ga	0.5	19	14	24	19	21	13	23	26
Zn	1	80	75	84	61	52	71	41	58
Ni	0.1	1082	826	1067	1121	1220	914	931	960
Mn	5	1091	1097	697	869	904	1136	979	882
Co	0.2	135	179	171	157	115	159	124	166

Note: *= Detection limit.

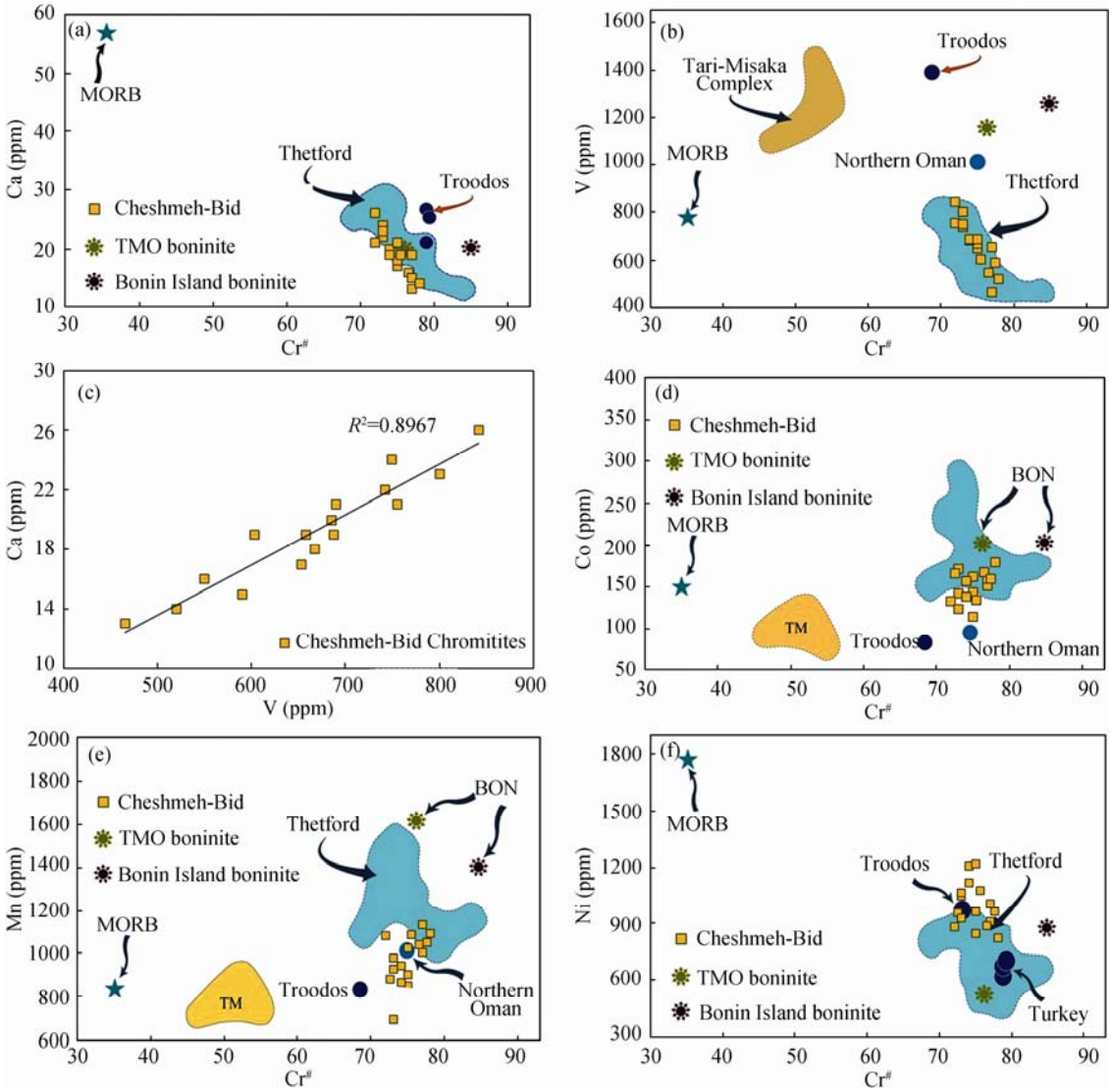

Fig. 9. $Cr^{\#}$ versus chromitite trace elements binary diagrams.
(a), $Cr^{\#}$ versus Ga; (b), $Cr^{\#}$ versus V; (c), $V^{\#}$ versus Ga; (d), $Co^{\#}$ versus Cr; (e), $Cr^{\#}$ versus Mn; (f), $Cr^{\#}$ versus Ni. Trace elements contents of the Cheshmeh-Bid deposit samples are similar to those of chromitites originating from boninitic magma. Thetford chromitite data from Page and Barnes (2009); Boninite and mid-ocean ridge basalt (MORB) data from Barnes and Roeder (2001); The Troodos chromitites (Paktunc and Cabri, 1995) and the northern Oman chromitites are from Arai and Yurimoto (1994).

9c). These data may be suggested that fractionation processes between chromitite and parental melt (Page and Barnes, 2009). Other trace elements such as Mn, Zn, Co, and Ni have variable values and vary between: 697 and 1136, 22 and 84, and 115 and 179, 826–1210 ppm, respectively, similar to chromites crystallized from boninitic magma (Fig. 9d−f,) (Table 5).

Trace elements contents of the Cheshmeh-Bid deposit samples are similar to those of chromitites originating from boninitic magma; Thetford chromitite data from Page and Barnes (2009); Boninite and mid-ocean ridge basalt (MORB) data from Barnes and Roeder (2001). The Troodos chromitites (Paktunc and Cabri 1995) and the northern Oman chromitites are from Arai and Yurimoto (1994).

6 Discussions

6.1 Parental melt composition of chromitites

Chromian spinel is a useful petrographic mineral and its composition record the chemistry of parental melt, the geodynamic setting in which the melts form, the source of peridotite, crystallization condition, the oxygen fugacity, the P-T condition of parental melt and the extent of reaction between parental melt and peridotite (Maurel and Maurel, 1982 and 1983; Roeder and Reynolds, 1991; Arai, 1992; Robinson et al., 1997). The chromian spinel compositions are a complex function of many factors; including magma composition (Maurel and Maurel, 1982), temperature (Scowen et al., 1991), pressure (e.g. Roeder and Reynolds, 1991; Lipin, 1993); f_{O2} (Roeder and

Reynolds, 1991) and SiO_2 (e.g. Irvine, 1975). Experimental data suggest that chromian spinel composition is sensitive petrogenetic indicator and provide important information to constrain the composition of parental melt within different geodynamic environments (e.g. Dick and Bullen, 1984; Melcher et al., 1999; Arai et al., 2004, 2006, 2011; Barnes and Roeder, 2001; Kamenetsky et al., 2001; Zhou et al., 2005; Rollinson, 2008; González-Jiménez et al., 2009, 2011; Pal, 2011). These experimental studies have also shown that parental melt for chromitites is the result of the melt-melt interactions or melt-rock reactions previously depleted in mantle sources in supra-subduction zone settings. On the based Xiong et al (2015a), the disseminated podiform chromitite formed at shallow depths under relatively low oxygen fugacity, in contrast, the massive and magnesiochromitite are considered to form at depth under high oxygen fugacity. Podiform chromitites formed as a result of the reaction between the primitive mantle and peridotite host rock of upper mantle (Robinson et al., 1997). High $Cr^{\#}$ chromitites formed at higher temperature and pressure than low $Cr^{\#}$ types, and H_2O has an important role by increasing partial melting (Mysen and Kushiro, 1977; Zhou and Robinson, 1994; Robinson et al., 2015). Partial melting of the rising peridotites at shallow mantle depths may cause redistribution of chromite grains and the formation of small chromitite pods (Yang et al., 2015). Based on $Cr^{\#}$ versus $Fe^{\#}$ binary diagram (Fig. 10a and b), it could be concluded that the high degree of partial melting (about 40%) required to deposit high $Cr^{\#}$ chromitites such as the Cheshmeh-Bid chromitites ($Cr^{\#}$ = 0.72–0.78 and $Fe^{\#}$ = 0.32–0.38).

In the $Cr^{\#}$ versus TiO_2 binary diagrams of Babien et al. (1998) (Fig. 10c), the study chromitites plot in the area of high $Cr^{\#}$(0.72–0.78) and low TiO_2 (0.20 wt%–0.33 wt%), reflecting crystallization from a boninite melt, whereas chromian spinel in harzburgite show an abyssal peridotite trend. Also, High $Cr^{\#}$ chomitite reported in Iranian podiform chromitites such as Neyriz, Sikhuran, Faryab, and Abdasht (Jannessray et al., 2012, Najafzadeh and Ahmadipour, 2014). The negative correlation between $Cr^{\#}$ and TiO_2 ($r = -0.64$) can be related to the different degree of mantle melting and differentiation of the parental melt. The TiO_2 content of chromitite decreases with increasing the degree of partial melting as a result of magma dilution (Kamenetsky et al., 2001; Maurel and Maurel, 1982).

It is well known that chromian spinel in chromitites inheritance their Al_2O_3 and TiO_2 content from the melt (Maurel and Maurel, 1982; Dick and Bullen, 1984; Arai, 1992; Roeder and Reynolds 1991, Barnes and Roeder, 2001). Therefore it could be used to determine the nature of parental melt and tectonic setting of chromitites by

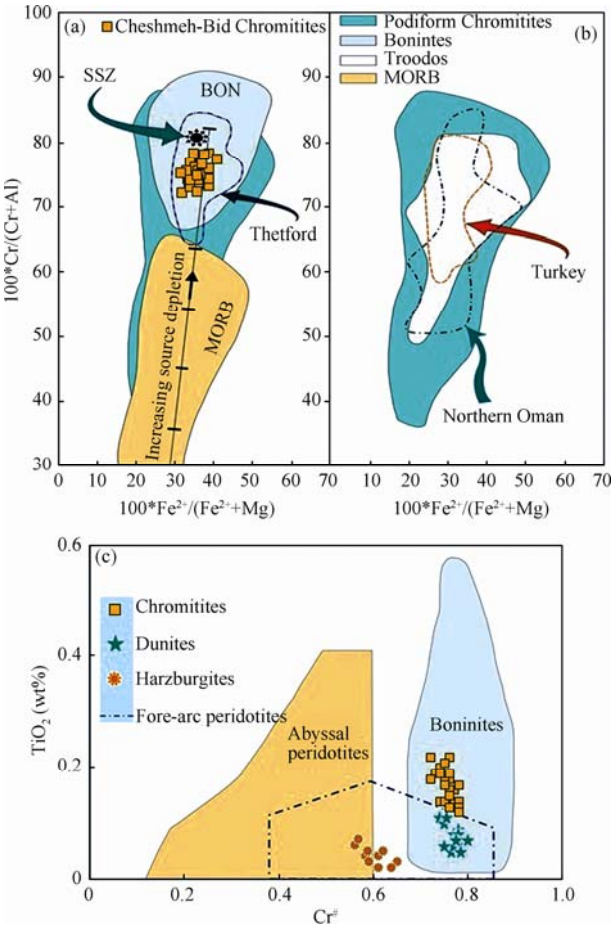

Fig. 10. Compares chromites from podiform chromitites of the Cheshmeh-Bid with samples from known settings.
(a), Variation of $Cr^{\#}$ versus $Fe^{\#}$ in chromites from chromitites of the Cheshmeh-Bid; (b), Shows subsets of the podiform chromitites compilation for comparison; (c), $Cr^{\#}$ versus TiO_2 chromian spinel of chromitite, dunite and harzburgite, showing fields of boninites for chromitite and dunite and abyssal peridotite for harzburgite (discrimination fields are after Tamura and Arai (2006)). Fields for midocean ridge basalt (MORB) and boninite (BON) (Barnes and Roeder, 2001); Thetford (Page and Barnes, 2009); Turkey (Paktunc and Cbri, 1995); Troodos and northern Oman (Arai and Yurimoto, 1994) are shown for comparison.

calculating Al_2O_3 and TiO_2 of primary melt because they are not affected by re-equilibration with interstitial melt or sulfides under the subsolidus condition, due to the proportion of olivine and interstitial melt is very low rather than chromite grains of chromitites. Accordingly, the geochemical composition of chromites as an important petrogenetic indicator is related to the compositions of their parental melt and can be used to calculate the Al_2O_3, TiO_2 and FeO/MgO ratios of the parental melt (Augé, 1987; Uysal et al., 2007, 2009)

The Al_2O_3 and FeO/MgO ratios of the primary parental melt can be calculated using the following equations of Maurel and Maurel (1982) and Maurel (1984) (cited in Augé, 1987), respectively:

$$(Al_2O_3\ wt\%)_{spinel} = 0.035(Al_2O_3\ wt\%)^{2.42}_{melt}$$

$$Ln(FeO/MgO)_{spinel} = 0.47–1.07Al^{\#}_{spinel} + 0.64Fe^{3+\#}_{spinel}$$

+ $Ln(FeO/MgO)_{melt}$

$Al^{\#} = Al/(Al + Cr + Fe^{3+})$

$Fe^{\#} = Fe^{3+}/(Al + Cr + Fe^{3+})$

However, by using these formulas, the Al_2O_3 and FeO/MgO ratios of the parental melts obtained for the melts in equilibrium with chromitites from the Cheshmeh-Bid are shown in Table 1.

Previous studies show that there is a linear relationship between the TiO_2 and Al_2O_3 contents of chromian spinel and the melt from which chromite crystallized (Kamenetsky et al., 2001; Rollinson, 2008). In the other words, the TiO_2 and Al_2O_3 values of chromian spinel correlate with those of the parental melt. The TiO_2 content of the parental melt in chromitites has been estimated using the regression lines from Zaccarini et al. (2011) using data from Rollinson (2008) and Kamenetsky et al. (2001) (Fig. 11a and b):

$TiO_{2\ melt}$ versus $TiO_{2\ spinel}$ regression lines:

Applying these formulas to the Cheshmeh-Bid chromitites show that Al_2O_3 and TiO_2 contents of the parental melt from which the chromitites crystallized for the high-Cr chromitites range between 11.53 wt%–12.94 wt% (12.23~) and 0.21–0.33 wt% (0.27~), respectively. The results indicate that FeO/MgO ratios of the parental melt of Cheshmeh-Bid chromitites vary between 0.69 and 0.97 (0.8~). The parental melt values of the Cheshmeh-Bid chromitites are compared with those of some well-known worldwide ophiolitic chromitites in Table 6. The $Al_2O_{3\ melt}$ and $TiO_{2\ melt}$ values of the Cheshmeh-Bid chromitites are similar to the High-Cr chromitites of Elekdağ in Turkey (Dönmez et al., 2014), N-Shitna in Iraq (Ismail et al., 2014), deep chromitites in Oman (Rollinson, 2008), Abdasht ophiolite in Iran (Najafzadeh and Ahmadipour, 2016), Nan Uttardite chromitites in Thailand (Orberger et al., 1995), and Bir Tuluha ophiolite in Saudi Arabia (Habtoor et al., 2017). In contrast, the FeO/MgO_{melt} values are similar to Soghan chromitites in Iran (Najafzadeh and Ahmadipour, 2016), Muğla in Turkey (Uysal et al., 2009), Sagua de Tanamo in Cuba (González-Jiménez et al., 2011), some Neoproterozoic ophiolitic complexes in Egypt (Ahmed, 2013); Al'Ays ophiolite-site 1 in Saudi Arabia (Ahmed and Habtoor, 2015), and Bir Tuluha ophiolite in Saudi Arabia (Habtoor et al., 2017) (Table 6). On the based previous studies (Najafzadeh et

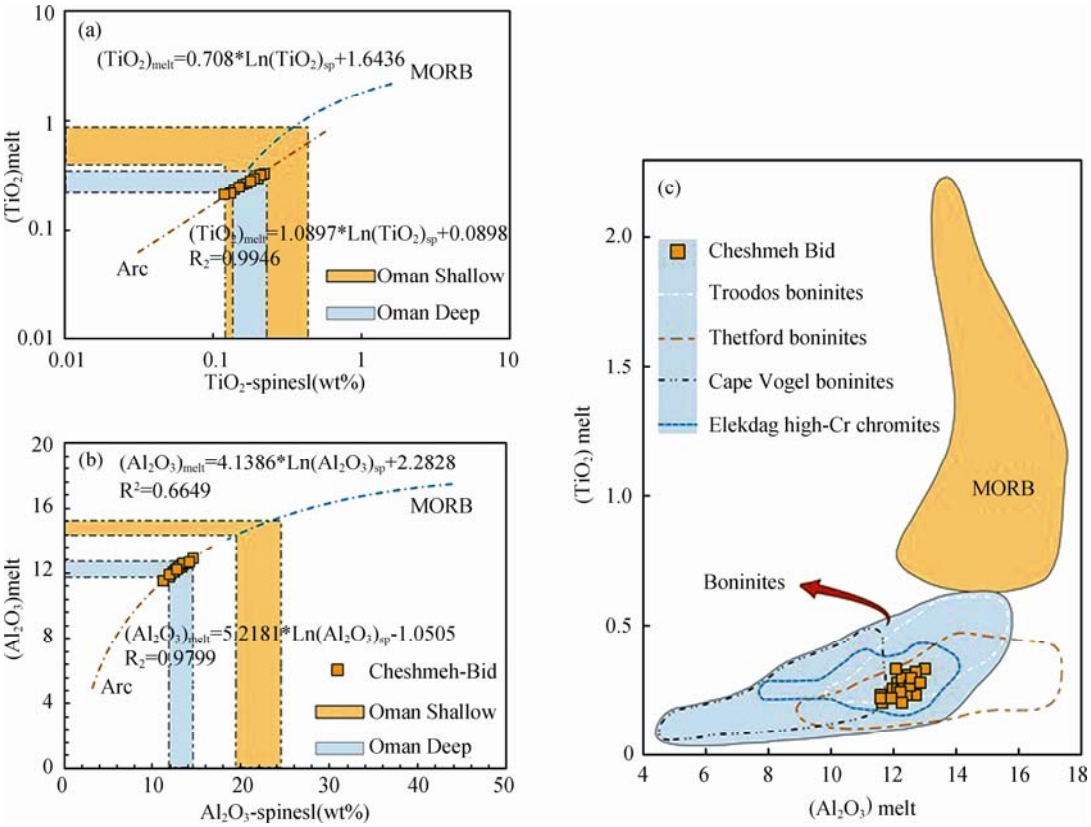

Fig. 11. Calculated $Al_2O_3$and TiO_2 values for the parental melts forming the chromitite in the Cheshmeh-Bid.
(a), TiO_2-melt (wt%) versus TiO_2-spinel (wt%) binary diagram; (b), Al_2O_3-melt (wt%) versus Al_2O_3-spinel (wt%) binary diagram. The regression lines for arc magma and MORB are based on Kamenetsky et al. (2001) and Rollinson (2008). Field of shallow and deep Wadi Rajmi chromitites in Oman (Rollinson, 2008). The range of chromian spinel and the calculated melt compositions from the Cheshmeh-Bid chromitites are shown as gray fields; (c), TiO_2-melt (wt%) versus Al_2O_3-melt (wt%), showing the Cheshmeh-Bid samples in the boninintc field (after Jenner, 1981; Walker and Cameron, 1983; Kamenetsky et al., 2002) and similar to the Thetford (Pages and Barnes, 2009), Troodos (Cameron, 1985), Elekdag (Donmez et al., 2014), and the Abdesht perdiote (Najafzadeh and Ahmadipour, 2016).

al., 2008; Jannessary et al., 2012., Rajabzadeh et al., 2013; Shafaii Moghadam et al., 2015., Soleimani and Jodeiri Shokri, 2016; Najafzadeh, and Ahmadipour, 2016), almost of Iranian podiform chromitite characterized by high Cr, dunite and harzburgite parent rock, boninitic magma, and supra subduction zone (SSZ) tectonic setting, except Nain and Shorkhband chromitites (Table 7).

Previous studies have shown that in ophiolitic complexes, Cr-rich chromitites tend to occur at the deeper parts of the upper mantle (Rollinson, 2008; Ismail et al., 2014). Peridotites hosting such Cr-rich chromitites are also more depleted than those hosting Al-rich chromitites (e.g. Leblanc and Violette, 1983; Proenza et al., 1999). The Cr-rich chromitites are crystallized from more refractory and similar to picritic and boninitic compositions (Zhou and Robinson, 1994). The composition of the parental melt from which the high-Cr chromitites of the Cheshmeh-Bid crystallized are similar to those of the chromitites formed in the deep mantle in the Oman Ophiolite (Rollinson, 2008; Arai et al., 2011)

Table 6 Comparison between the parental melt composition of the Cheshmeh-Bid chromitites and other worldwide high-Cr podiform chromitites

Complex	$Cr^{\#}$	Al_2O_3 (spinel)	Al_2O_3 (melt)	TiO_2 (spinel)	TiO_2 (melt)	FeO/MgO (melt)	Reference
Neoproterozoic ophiolitic complexes (Egypt)	0.77–0.91	4.4–12.21	8.49−12.71	0.03–0.13	−	0.67–1.88	Ahmed (2013)
Bou Azzer ophiolite (Anti-Atlas, Morocco)	0.64–0.77	11.75−20.16	−	0.05−0.1	−	−	Ahmed et al. (2009)
Al'Ays ophiolite- site 1 (Saudi Arabia)	0.85–0.86	6.75–7.13	8.51–9.02	0.06−0.07	0.00–0.06	0.57–0.63	Ahmed and Habtoor (2015)
Bir Tuluha ophiolite (Saudi Arabia)	0.72–0.81	9.68–15.04	10.21–12.29	0.09−0.16	0.17–0.28	0.61–0.79	Habtoor et al. (2017)
Pan-African Proterozoic Ophiolite complexes (Egypt)	0.5–0.86	5.72–29.77		0.04−0.4			Ahmed et al. (2001)
Abadeh Tashk (Iran)	0.73–0.81	0.73–0.81	10.48−12.66	0.02–0.08	0.05−0.15	0.71–1.04	Rajabzadeh et al. (2013)
Abdasht chromitites (Iran)	0.76–0.77	12.00–12.80	11.92–12.25	0.14–0.20	0.23–0.31	0.60–0.65	Najafzadeh and Ahmadipour (2016)
High-Cr chromitites (Eastern Cuba)	0.63–0.72	16.30	13.40	0.19	0.30	0.90–1.50	González-Jiménez et al. (2011)
N-Shitna high-Cr chromitite (Iraq)	0.76−0.82	10.37–12.13	8.92−12.51	0.09−0.13	0.17−0.22	0.60–0.73	Ismail et al. (2014)
Berit ophiolite (Turkey)	0.64−0.79	10.19−17.16	11.06−13.78	0.11−0.19	0.19–0.30	−	Kozlu et al. (2014)
Elekdağ ophiolite (Turkey)	0.65–0.89	5.10–18.20	9.40–13.20	0.14–0.26	0.20–0.40	0.40–1.90	Dönmez et al. (2014)
Deep chromitites (Oman)	0.71–0.77	11.70–14.40	11.80–12.90	−	0.23–0.34	−	Rollinson (2008)
Boninite	−	−	11.29–14.87	−	0.22–0.24	0.68–0.89	Falloon et al. (2008)
Cheshmeh-Bid (Iran)	0.72–0.78	11.15–14.61	11.53–13.79	0.12–0.22	0.2–0.33	0.69–0.97	This study

Table 7 Comparison between the petrological and geochemical characteristics of the Cheshmeh-Bid chromitites and other Iranian podiform chromitites.

Complex	Mine/prospect	Age	Parent rock	Parent magma	Tectonic setting	$Cr^{\#}$	Reference
Sorkhband	Sorkhband	Ordovician	Dunite, harzburgite	Boninite, MORB	SSZ	0.75−0.89	Najafzadeh et al (2008)
Neyriz	Khajeh-Jamali	Late Cretaceous	Dunite	Boninite	SSZ	0.73−0.80	Jannessary et al. (2012)
Neyriz	Tang-e-Hana	Late Cretaceous	Dunite	Boninite	SSZ	0.60−0.70	Jannessaryet al. (2012)
Abdasht	Soghan	Late Cretaceous	Dunite	Boninite	SSZ	0.60−0.85	Najafzadeh, and Ahmadipour, (2016)
Esfandagheh	Sikhuran	Paleozoic	Dunite	Boninite	SSZ	0.75−0.82	Jannessary et al. (2012)
Faryab	Reza	Ordovician?	Serpantized dunite	–	–	0.78−0.82	Jannessary et al. (2012)
Nain	Hossein Abad, Soheil Pakuh	Late Cretaceous	Dunite, harzburgite	MORB	Back-arc	0.59−0.73	Rajabzadeh et al. (2013)
Sabzevar	Forumad	Late Cretaceous	Harzburgite	Boninite	SSZ	0.77–0.83	Soleimani and Jodeiri Shokri (2016), Shafaii Moghadam et al. (2015)
Sabzevar	Baghjar-Kuh Siah	Late Cretaceous	Lherzolites	MORB	Fore-arc	0.34−0.45	Shafaii Moghadam et al. (2015)
Sabzevar	Gaft	Late Cretaceous	Harzburgite	Boninite	SSZ	0.77–0.78, 0.41–0.43	Shafaii Moghadam et al. (2015)
Cheshmeh-Bid	Cheshmeh-Bid	Late Cretaceous	Dunite, harzburgite	Boninite, MORB	SSZ	0.72–0.78	This study

(Fig. 11a and b), and can be interpreted as more refractory melts akin to boninitic compositions (10.6 wt%–14.4 wt% Al_2O_3, 0.7–1.4 FeO/MgO) (Fig. 10; Table 5). These chromitites have relatively higher $Cr^{\#}$ and lower TiO_2 and Al_2O_3 contents compared to high-Al chromitites formed closer to MOHO discontinuity (Fig. 11). The $TiO_{2\ melt}$ (wt%) versus $Al_2O_{3\ melt}$ (wt%) binary diagram (Page and Barnes, 2009) of the Cheshmeh-Bid chromitite indicates that parental melt is boninitic in composition (Fig. 11c). These estimates for the parental melts show that the compositions of the chromian spinel in the Cheshmeh-Bid chromitites are indicative of crystallization from melts derived from the depleted mantle. The high-Cr chromitites from the Cheshmeh-Bid plot in the primitive mantle fields and indicate strong affinity with melts from depleted mantle and boninites similar to Elekdağ high-Cr chromitites (Dönmez et al., 2014), Thetford boninites (Pagé and Barnes, 2009), Troodos boninites in Cyprus (Flower and Levine, 1987), and Cape Vogel boninites in Guinea (Walker and Cameron, 1983) (Fig. 11c).

According to our investigations, the origin of the Cheshmeh-Bid chromites can be explained by melt-rock reaction model. The dunite enveloping chromitite pods is a good evidence for the melt-peridotites interaction model, where the temperature in the mantle wedge is too low to form dunite solely by partial melting of the mantle (Ahmed and Habtoo, 2015). This model has already been proposed by Arai and Yurimoto (1994), Zhou et al. (1996) and Rollinson (2005, 2008); and implies that primary mafic melts reacted with mantle harzburgite whereas ascending through the shallow upper mantle, dissolving orthopyroxene and leaving a residue of dunite (Ismail et al., 2014; Robinson et al., 2015). The dissolution of orthopyroxene drives the melt toward a boninitic or high-Mg andesitic composition and moves it into the field of chromite crystallization (Kelemen et al., 1992; Irvine, 1977). The High $Cr^{\#}$ in chromian spinel, and depleted in PPGE, implies that either a high degree of partial melting or a partial melting of an already depleted mantle peridotite. This also implies that chromitite forming magma was originally highly S-undersaturated (e.g. boninitic magma) to be able to dissolve the mantle sulfides and partly removed the Pd and Pt resident in their mantle host rocks (Ahmed et al., 2009).

6.2 The geochemical signature of the trace and platinum-group elements

PGE in ultramafic melts is released from mantle sources as a result of different partial melting of sulfide or PGE alloy minerals. Only a few of podiform chromitites have enriched in PGE; however, their total PGE contents are few to be economically extracted (Economou-Eliopoulos, 1996; Prichard et al., 1996; Ohnenstetter et al., 1991). A critical melting stage (Twenty to twenty-five percent of mantle melting) would be necessary in order to release large amounts of PG elements into mantle melts. The release of sufficient PGE into the melt will in a narrow range of melting. Increasing melting percentages result in dilution of the PGE and lower degree of partial melting caused most of these elements remains in the sulfides of the residuum (Naldrett et al., 1979; Hamlyn et al., 1985; Hamlyn and Keays, 1986; Naldrett and von Gruenewaldt, 1989; Rehkämper et al., 1999; O'Hara et al., 2001a, b; Mungall, 2005; Prichard et al., 2008).

The most Iranian chromitite are characterized by low to moderate total PGE content, that hardly exceeds of 500 ppb, and Pt and Pd contents are very low (Jannessary et al., 2012). This is in the range of Alpine-type ophiolitic chromitite, (e. g. Ahmed and Arai, 2002, Econmou-Eilpoulos, 1996; Kock et al., 2007, Uysal et al 2010). The Cheshmeh-Bid chromitite is characterized by high $Cr^{\#}$ (average of 0.75), low PGE content (average = 220.34), and a systematic enrichment in IPGE (Os, Ir, Ru) relative to PPGE (Rh, Pt, Pd) (Table 4), a feature typical of the worldwide ophiolitic podiform chromitites. Kozlu et al. (2014) believed that if chromitites were formed by a fractionation from an originally high-chromian melt, therefore the PGE mineralization is related to a high degree of fractionation and a higher degree of partial melting, the reverse relationship can be deduced from high Al chromitite. Chondrite-normalized PGE patterns for the Cheshmeh-Bid chromitites with general negatively sloping patterns are similar to those of mantle-derived podiform chromitites formed in supra-subduction zones worldwide (Figs. 7a and b) (Melcher et al., 1999; Ahmed and Arai, 2002; Garuti et al., 2005; Başpınar, 2006; Akbulut et al., 2010; Dönmez et al., 2014; Ismail et al., 2014; Najafzadeh and Ahmadipour, 2016; Economou-Eliopoulos et al., 2017). The relative enrichment of IPGE in chromitite samples is reflected by highly negative slopes from Ru to Pt. These patterns and the low PGE abundances are typical of chromitites in ophiolites from elsewhere (Such as Abdasht; Faryab; N Shitna; Elekdag high-Cr and Luobusa ultra-high pressure chromitites) (e.g. Rajabzadeh et al., 1988; Uysal et al., 2009; Dönmez et al., 2014; Ismail et al., 2014; Najafzadeh and Ahmadipour, 2016). The high-Cr chromitite are as a result of S-under saturated boninitic magma that reacted with depleted harzburgite at a deeper level (Zhou et al., 1998, Ismail et al., 2014). Chondrite-normalized PGE patterns show slightly positive Ru and strongly negative Pt anomalies (Fig. 7). As stated by many authors (Bacuta et al., 1990; Ismail et al., 2014) PPGE (especially Pt), behave as more incompatible elements than the other IPGE during hydrous partial melting in a

supra-subduction zone and therefore enriched in later fractionate as Pt-Fe alloy, causing a strongly negative Pt-anomaly in early formed chromitites.

Previous studies suggest that the enrichment of PGE can be controlled by the presence of magmatic sulfides accompanied by chromite or PGE during fractionation (Cina et al., 2002). However, chromitite, dunite and harzburgite samples in the Cheshmeh-Bid deposit have a wide range of Pd/Ir values (0.05 to 0.18 in chromitites, 3.2 to 3.5 in dunite, and 2.8 to 4.0 in harzburgite) such as the Abdasht ultramafic complex (Najafzadeh and Ahmadipour, 2016) and Elakdag ophiolite (Donmez et al., 2014), which reflect variations in the amounts of partial melting rather than magmatic fractionation (Naldrett et al., 1979; Page et al., 2008) (Table 4; Fig. 12). The preferential concentration of the extracted PPGE in silicate melts during partial melting, while the mantle residue is enriched in IPGE, may explain the decrease of the Pd/Ir ratio with increasing partial melting degree in the mantle peridotites of ophiolites (Garuti et al., 1997; Melcher et al., 1997; Uysal et al., 2009; Economou-Eliopoulos et al., 2017). Based on Economou-Elipoulos et al. (2017), the large chromite deposits exhibit Pd/Ir<1 and negative Pt/Pt* values, which reflect partial melting of the already depleted mantle. Also, it is believed that difference in the Pd/Ir ratio is considered as an index of fractionation degree of the PGE during the petrological process (Barnes et al, 1985). Accordingly, the low Pd/Ir and Pt/Pt* values suggesting that the parent magma exhibits a very low fractionation degree and was derived by an increasing partial melting degree (Economou-Eliopoulos et al., 2017). On the based Pd/Ir versus Pt/Pt* diagram, the Cheshmeh-Bid chromitite indicate a partial melting trend (Fig. 12). Pd/Ir ratios (0.05−0.18) for the chromitites from the Cheshmeh-Bid are significantly lower than values for the average mantle, and show that derived from a depleted mantle where IPGE crystallize and are left out from the melt whereas other PGEs remain in residual melt (e.g. Garuti et al., 1997; Dönmez et al., 2014). As illustrated in Table 4, dunites and harzburgites in the Cheshmeh-Bid ophiolite are depleted in PGE relative to the associated chromitites, while enriched relative to the upper mantle (McDonough and Sun, 1995). The dunites from the Cheshmeh-Bid Ophiolite have similar chondrite-normalized PGE patterns to harzburgites and are relatively flat but indicate weakly negative Ir and Rh anomalies (Fig. 7b). In addition, there are some negative Pt anomalies (Ch-D-3 and Ch-H-2 samples) for peridotites. The trend shows that Pt behaves as incompatible elements during mantle partial melting, although it is depleted to an appreciable extent only at relatively high degrees of melting when residual dunites are produced (Garuti et al., 1997). Both the dunites and harzburgites are somewhat richer in PPGE than in IPGE (Table 4).

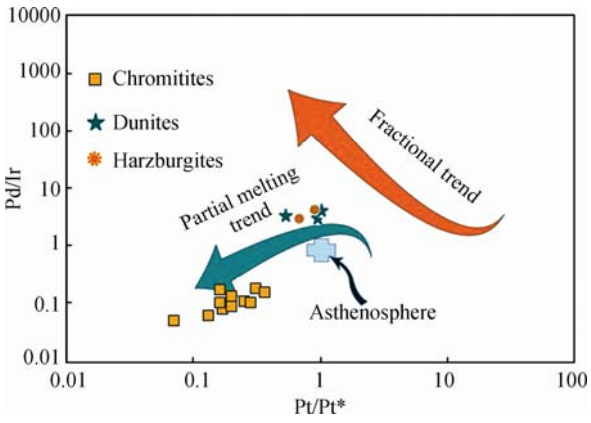

Fig. 12. The plot of platinum anomaly (Pt/Pt*) versus Pd/Ir in chromites and peridotites from the Cheshmeh-Bid. The Cheshmeh-Bid samples indicate a partial melting trend.
Fractional and partial trends are from Grauti et al. (1997).

Despite the economic significance of PGE, it still remains ambiguous how PGE are mobilized distributed and transported in the mantle and subsequently become enriched in chromitites as part of the ophiolite. Some researchers (Brenan and Andrews, 2001; Andrews and Brenan, 2002) believe that the partial melting, temperature, and sulfur fugacity are the most important controlling factors in the deposition of sulfides or alloys of PGE (especially Ru-Ir-Os). IPGM as primary inclusion in chromitite, are controlled by fS_2 and temperature of magma (Eonomou-Elipoulos et al., 2017). Accordingly, the difference in sulfur saturation in boninitic and tholeiitic melts determines PGEs contents in chromitites (Prichard et al., 1996). Boninite-like melts are commonly unsaturated in sulfur and formed by the partial melting of an excessively depleted mantle source at high grade (≥20%) hence, there is approximately a positive relationship between the degree of partial melting, and the PGEs contents and $Cr^{\#}$ (Zhou et al., 1998; Prichard et al., 2008; Dönmez et al., 2014). The mostly inverse relationship of higher $Cr^{\#}$ and lower PPGE content can be interpreted in two ways depending on the nature of chromium and alumina spinel formation (Kozlue et al., 2014). In the high $Cr^{\#}$ chromitite, IPGE content is related to the high degree of partial melting, whereas the strong depletion in PPGE and decoupling between IPGE and PPGE in high-Cr chromitite is related to the differences in melting point of these elements during partial melting (Ahmed and Arai, 2002). The IPGE with high melting points tend to be retained in high-Cr chromitite at high degrees of partial melt, whereas PPGE with lower melting points tend to be retained in the residual melt, which will precipitate at shallow level in the ophiolitic sequences and

mainly associated with sulfides in gabbros and transition dunites (Ahmed and Arai, 2002). Instance, the Tang-Hana small podiform chromitite (northern part of the Neyriz ophiolite), has higher PGE content (average= (1556 ppm) and lower $Cr^{\#}$ than the Cheshmeh-Bid deposit (Jannessary et al., 2012). In fact, removal of sulfide minerals prior to chromitite formation and high-degrees of partial melting, lead to leaching of PPGE from the peridotite unites and transferring them into the S under-saturated magmas, leaving a mantle residue highly depleted in these elements (e.g. Zhou et al., 1998; Ismail et al., 2014; Najafzadeh and Ahmadipour, 2016). This type of magmas is derived from a supra-subduction zone setting. Generally, in supra-subduction zone environments, the partial melting grad is much higher than in mid-ocean ridge settings. In these geodynamic settings peridotites have been highly depleted and metasomatized and the partial melting has been done under hydrous conditions (Arai and Matsukage, 1998; Ahmed and Arai, 2002). This stage of the partial melting will leave behind a podiform chromitite notably enriched in Cr and IPGE and highly depleted in PPGE (e.g. Zhou et al., 1998; Büchl et al., 2004; Grammatikopoulos et al., 2011).

The high-$Cr^{\#}$, low Pd + Pt and high IPGE/PPGE ratios in the Cheshmeh-Bid chromitites suggesting that a high-degree of partial melting was responsible for the formation of the Cheshmeh-Bid chromitites. These characteristics show that the chromitites were crystallized from boninitic melts in a supra-subduction setting similar to the podiform chromitites from the Qalander ophiolite in Iraq (Ismail et al., 2014). In addition, these geochemical features also implies that the Cheshmeh-Bid chromitites have been probably derived from an S under-saturated boninitic magma that reacted with depleted peridotites and has been able to dissolve the mantle sulfides and that Pt and Pd were partly removed either before or during chromitite formation (Zhou et al., 1998; Garuti, 2004; Uysal et al., 2009; Zaccarini et al., 2011; González-Jiménez et al., 2011).

Trace elements composition of the Cheshmeh-Bid chromitite samples shows that depletion of Ga and V compared to MORB reflects more reducing conditions or more oxidation conditions during ascending of boninitic magma from a higher depth to shallower parts. Titanium, Ga, Ni and V contents of chromites from podiform chromitites in the Cheshmeh-Bid mine show relatively negative correlations with $Cr^{\#}$ (Fig. 9). It suggests that boninitic magmas are clearly depleted in the Ga, V, Ti, and Ni in contrast to MORB magmas (Fig. 9). Also, negative correlation between $Cr^{\#}$ and Ga; suggest that Ga abundances are controlled by the distribution of trivalent cations (Zhou et al., 2014). Based on Page and Barnes (2009) contents of Zn, Al, Mn, Ti, V, Ga, and Co are mainly controlled by chromite crystallization, but Ni and Mg mainly by olivine. Ni, Ga, Al contents are useful for distinguishing boninitic chromite from MORB chromite.

6.3 Implications for the geodynamic setting

The Neyriz Tectonic setting is an immature island arc (Shahabpour, 2005) that developed above a subduction zone during the Jurassic and Cretaceous. A steep subduction angle is indicated by the presence of Jurassic-Cretaceous subduction-related, calc-alkaline volcanic and plutonic rocks in the Sanandaj-Sirjan zone and the absence of such rock types in the Uromieh-Dokhtar magmatic belt (Berberian and Berberian, 1981; Shahabpour, 2005, Ghazi et al., 2010).

The chemical composition of chromite acts as a conservative index and can be used to constrain the parent melt composition and tectonic settings (e.g. Dick and Bullen, 1984; Arai, 1992; Zhou et al., 1996; Kamenetsky et al., 2001; Page and Barnes, 2009). The field observations and the geochemical features of chromitite and associated ultramafic rocks were used to discriminate the tectonic setting of the Cheshmeh-Bid area. The geological, petrographical and geochemical complexity of ophiolitic podiform chromitites in different tectonomagmatic environments has been discussed for over two decades (Melcher et al., 1997; Zhou and Robinson, 1997; Zhou et al., 1998; Malitch et al., 2003; Büchl et al., 2004; Gervilla et al., 2005; Robinson and Zhou, 2008; Ismail et al., 2014; Dönmez et al., 2014; Kozlue et al., 2014; Najafzadeh and Ahmadipour, 2016). These studies show that chromitite formation may occur in the upper mantle as ‘stratiform’ and ‘podiform’ types both in the ultramafics and also at the crust-mantle transition zone. However, it is now widely accepted that most ophiolitic podiform chromitites contain geochemical signatures indicative of their formation in supra-subduction zone environments (Robinson and Zhou, 2008). Based on Kocks et al. (2007), fluxing of previously depleted peridotites by hydrous fluids and/or melts within SSZ environments results in chromium and PGE-rich melts that are able to migrate out of their source region.

Based on the geochemical characteristics of chromian spinel, two groups of data can be recognized: (1) chromian spinel from chromitites and associated dunite envelopes, and (2) chromian spinel from harzburgite host. The average Cr-ratios in chromian spinel of chromitites and dunite envelopes are 0.75 (0.72–0.78) and 0.76 (0.73–0.8), respectively. The average Cr-ratio of chromian spinel in harzburgite host is distinguishable from the earlier ones; it is 0.6 (0.56–0.65) (Tables 1 and 2). Harzburgite, which is the main mantle lithology in the Cheshmeh-Bid ophiolite,

is the most common host for podiform chromitites in ophiolites of different tectonic settings and ages (Arai, 1997), and it is the most common lithology in the ophiolitic mantle section worldwide (Ahmed and Arai, 2002; Le Mee et al., 2004; Habtoor et al., 2017). The intermediate average Cr-ratio of chromian spinels and the low PGE contents with approximately unfractionated patterns (Fig. 7b) of the studied harzburgite host suggest a mantle residue after a low degree of partial melting at MOR setting (Habtoor et al., 2017). It is highly possible, therefore, that the harzburgite host of the Cheshmeh-Bid was derived from the ophiolitic upper mantle section produced at an MOR environment. This is supported by the Al_2O_3-TiO_2 binary diagram (Fig. 13a), where all the analyzed chromian spinels from harzburgite are entirely plotted within the MOR peridotite field. Kamenetsky et al. (2001) believed that the TiO_2 and Al_2O_3 compositions of chromian spinel are key factors in determining different tectonic settings. The TiO_2 content of the Cheshmeh-Bid chromitite (average of 0.17), dunite (average of 0.08) and harzburgite (average of 0.04) is very low. As illustrated in Fig. 13a, chromian spinel compositions of the chromitites and dunites from the Cheshmeh-Bid are a plot in the arc and supra-subduction zone fields. In addition, in TiO_2 versus Fe_2O_3 binary diagram, all of the samples indicate supra-subduction zone ophiolites (Fig. 13b). Parental magma compositions of high-Cr chromitites were probably formed as a result of the interaction of boninitic melts and peridotites of various degrees of depletion. (Rollinson, 2008; González-Jiménez et al., 2011). Such types of melt-rock interaction patterns show that the Cheshmeh-Bid chromian spinels most likely occurred in the fore-arc tectonomagmatic environment (Parkinson and Pearce, 1998; Okamura et al., 2006). The high $Cr^{\#}$ values and low TiO_2 and Al_2O_3 content of the Cheshmeh-Bid high-Cr chromitites suggest that these chromitites were likely formed in the mantle beneath a fore-arc setting related with a supra-subduction zone (Fig. 13c). The high-Cr chromitites are poor in PGE content (average of 220 ppb, Table 4) and PGM. Low Pd/Ir and high IPGE/PPGE ratios (average of 0.11 and 12.11, respectively) reveal higher degrees of partial melting in a supra-subduction zone.

Ophiolites from the Zagros Suture Zone can be divided in two the parallel belts as the outer and inner Zagros ophiolitic belts. The Cheshmeh-Bid ophiolite from the outer belt shows remnants of the southern branch of the Neo-Tethyan Ocean in Iran. Some researchers, in terms of

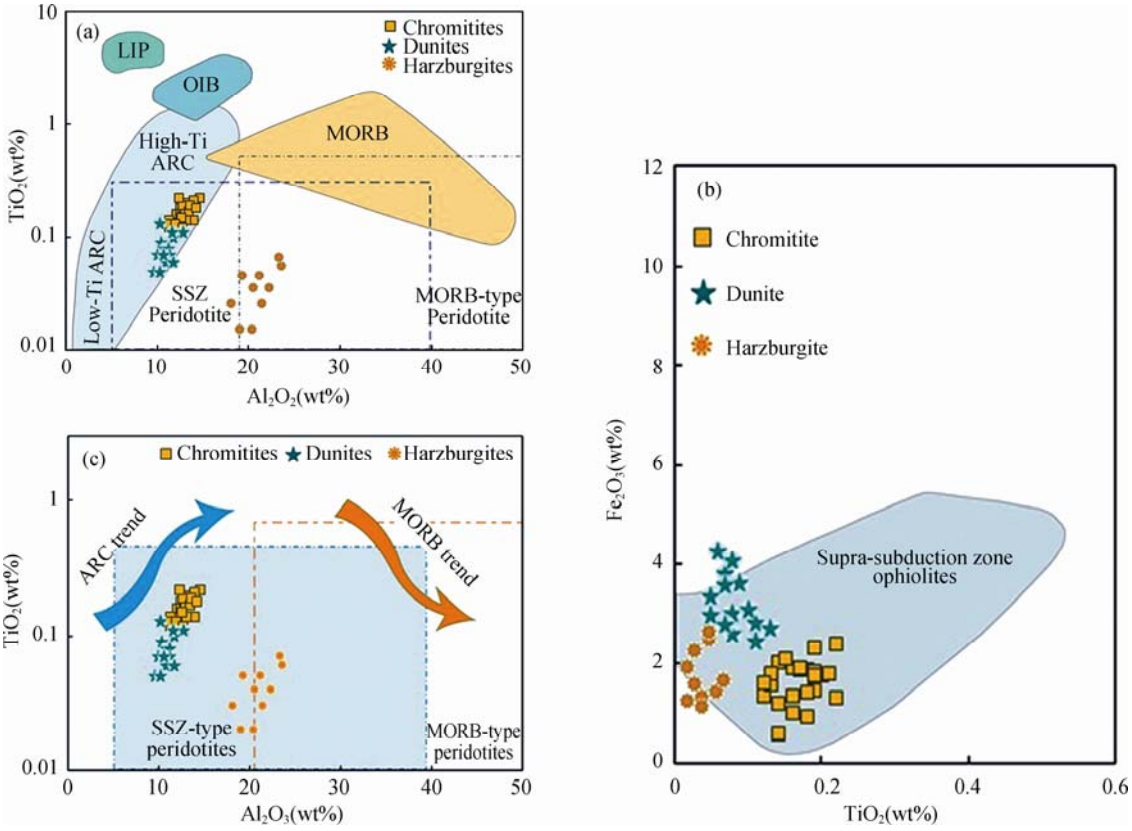

Fig. 13. Tectonic discrimination diagrams for chromitites from the Cheshmeh-Bid.
(a), Spinel- Al_2O_3 versus Spinel-TiO_2 distribution diagram of the Cheshmeh-Bid samples plotted (after of Kamenetsky et al., 2001); (b), Plot of TiO_2 versus Fe_2O_3 of chromian spinels of Cheshmeh-Bid chromitite (after of Bridges et al., 1995); (c), Plot of Al_2O_3 versus TiO_2 in chromian spinels from the Cheshmeh-Bid chromitite (after Kamenetsky et al., 2001).

the geochemical characteristics of the ultramafic rocks and mineral chemical compositions of peridotites and chromitites from the inner and outer belt ophiolites suggested that the back-arc and island-arc settings are the most widely-recognized settings for the formation of podiform chromitites, respectively (Shafaii Moghadam and Stern 2011a,b; Ghazi et al., 2010, 2011). In these settings, chromitites probably have been formed by melt/rock interaction in the upper mantle (Zhou and Bai, 1994). Several pieces of evidence such as the existence of high-Cr chromitites, boninitic magmas, the low TiO_2 and chromian spinel compositions of both chromitite and peridotites suggest a fore-arc tectonic setting for the Cheshmeh-Bid, similar to other ophiolites in the outer Zagros ophiolitic belt.

High degrees of partial melting resulted in high $Cr^{\#}$ and lower titanium and PGE content in chromitites of the study area. The model proposed for the genesis of the Neyriz chromitites is similar to that of other chromitite occurrences along the Zagros thrust belt, such as those at the Haji-Abad Esfandagheh (Najafzadeh and Ahmadipour, 2016) and Fariab (Jannessary et al., 2012), in northern Iraq (Ismail et al., 2010) and the Khoy ophiolites (Imamali Pour, 2011), which may reflect similar conditions of formation during subduction of the Neo-Tethyan margin (Tables 6 and 7).

7 Conclusions

Based on petrographical, mineralogical and geochemical studies of the Cheshmeh-Bid chromitite and their host rocks, the following conclusions can be deduced:

(1) The mantle peridotites hosting the Cheshmeh-Bid chromitites are serpentinized harzburgites with less abundant dunites. Olivine composition in the Cheshmeh-Bid harzburgite and dunite is highly forsterite (Fo>90%) with little variation.

(2) The podiform Cheshmeh-Bid chromitites have $Cr^{\#}$ > 0.7, low% TiO2 (0.17), and $Fe^{\#}$ and $Mg^{\#}$ similar to those of boninitic chromitites. The Al_2O_3, TiO_2 contents and FeO/MgO ratio of the parental melt for the Cheshmeh-Bid chromitites range from 11.53 wt% to 12.94 wt%, 0.21 wt% to 0.33 wt% and 0.69 to 0.97, respectively. The composition of the parental melt from which the high-Cr chromitites of the Cheshmeh-Bid crystallized is more refractory melts akin to boninitic compositions.

(3) The composition of chromian spinels in chromitites (ave. ~0.75) and dunite (ave. ~0.76) envelopes shows little variation, which is quite different from those in the harzburgite host (ave. ~0.6). The high Cr-ratio of chromian spinels in chromitites and associated dunite envelopes along with very low TiO_2 content, suggests their formation by the interaction between MOR mantle harzburgite with arc-related magma.

(4) Total PGE content of the Cheshmeh-Bid chromitite, dunite and harzburgite are very low (average of 220.4, 34.5, and 47.3, respectively). The Cheshmeh-Bid samples are enriched in Ir-group and depleted in the Pt-group (SIPGE/SPPGE = 0.8.20–22.25). High degrees of partial melting caused dilution of PGE in the primary magma resulting in decreasing contents of PGE. The Low Pd/Ir ratios show that the chromitites from the Cheshmeh-Bid derived from a depleted mantle where IPGE crystallize and were left out from the melt whereas other PGEs remain in residual melt. The high IPGE/PPGE ratios, negative Pt/Pt^{*} values, low Pd/Ir ratio in the Cheshmeh-Bid chromitites probably reflect that the parent magma exhibit a very low fractionation degree and was derived by an increasing partial melting degree. These geochemical characteristics suggest that the Cheshmeh-Bid chromitites have been probably derived from an S under-saturated boninitic melt in a supra-subduction setting that reacted with depleted peridotites and have been able to dissolve the mantle sulfides and that Pt and Pd were partly removed either before or during chromitite formation.

(5) The evidence mentioned above suggest a fore-arc tectonic setting related with a supra-subduction zone for the Cheshmeh-Bid, similar to other ophiolites in the outer Zagros ophiolitic belt. A steep angle of subducting Neothetys ocean crust at this time resulted in high degree partial melting and the production of hot water-rich melts from which chromite precipitated during ascent.

Acknowledgements

The authors are grateful to the research committee of Shiraz University for supporting this project. We would like to give our sincere thanks to Dr. Martin J. Timmerman of the Universität Potsdam for reviewing an earlier version of the manuscript and constructive comments. Thanks are extended to Prof. Maria Economou -Eliopoulos (National and Kapodistrian University of Athens) and two anonymous reviewers for critical review and constructive comments to improve the manuscript. The authors would like to express their thanks to Dr. İbrahim Uysal of Karadeniz Technical University (Trabzon, Turkey) for very useful comments, Mostafa Nejadhadad, Maryam Javid and Parvin Rahimi (Shiraz University) for their kindly help in this research. We are grateful to Prof. Degan Shu and Prof. Lian Liu, Editors-in-chief of Acta Geologica Sinica-English Edition for the editorial handling of the manuscript and constructive comments.

Manuscript received Jun. 2, 2017
accepted Jul. 25, 2017
edited by Liu Xinzhu

References

Ahmed, A.H., and Arai, S., 2002. Unexpectedly high PGE chromitite from the deeper mantle section of the northern Oman ophiolite and its tectonic implications. *Contribut. Mineral. Petrol.*, 143(3): 263–278.

Ahmed, A.H., Arai, S., Abdel-Aziz, Y.M., Ikenne, M., and Rahimi, A., 2009. Platinum-group elements distribution and spinel composition in podiform chromitites and associated rocks from the upper mantle section of the Neoproterozoic Bou Azzer ophiolite, Anti-Atlas, Morocco. *J. African Earth Sci.*, 55(1): 92–104.

Ahmed, A.H., Harbi, H.M., and Habtoor, A.M., 2012. Compositional variations and tectonic settings of podiform chromitites and associated ultramafic rocks of the Neoproterozoic ophiolite at Wadi Al Hwanet, northwestern Saudi Arabia. *J. Asian Earth Sci.*, 56(1): 118–134.

Ahmed, A.H., and Habtoor, A., 2015. Heterogeneously depleted Precambrian lithosphere deduced from mantle peridotites and associated chromitite deposits of Al'Ays ophiolite, Northwestern Arabian Shield, Saudi Arabia. *Ore Geol. Rev.*, 67: 279–296.

Akbulut, M., Pişkin, Ö., Arai, S., Özgenç, I., and Minareci, F., 2010. Base metal (BM) and platinum-group elements (PGE) mineralogy and geochemistry of the Elmaslar chromite deposit (Denizli, SW Turkey): implications for a local BM and PGE enrichment. *Ofioliti*, 35(1): 1–20.

Alavi, M., 1994. Tectonics of Zagros Orogenic belt of Iran, new data and interpretation. *Tectonophysics*, 229(3−4): 211–238.

Andrews, D.R.A., and Brenan, J.M., 2002. Phase equilibrium constraints on themagmatic origin of laurite+Ru-Os-Ir alloy. *Canadian Mineral.*, 40(6): 1705–1716.

Arai, S., 1992. Chemistry of chromian spinel in volcanic rocks as a potential guide to magma chemistry. *Mineral. Magazine*, 56: 173−184.

Arai, S., 1994. Characterization of spinel peridotites by olivine-spinel compositional relationships: Review and interpretation. *Chemical Geol.*, 113: 191–204.

Arai, S., and Yurimoto, H., 1994. Podiform chromitites of the Tari-Misaka ultramafic complex, southwestern Japan, as mantle-melt interaction products. *Economic Geol.*, 89: 1279−1288.

Arai, S., 1997. Origin of podiform chromitites. *J. Asian Earth Sci.*, 15(2−3): 303−310.

Arai, S., Uesugi, J., and Ahmed, A.H., 2004. Upper crustal podiform chromitite from the Northern Oman ophiolite as the stratigraphically shallowest chromitite in ophiolite and its implication for Cr concentration. *Contribut.Mineral. Petrol.*, 147: 145–154.

Arai, S., Kadoshima, K., and Morishita, T., 2006. Widespread arc-related melting in the mantle section of the northern Oman ophiolite as inferred from detrital chromian spinels. *Geol. Soc. London*, 163: 869–879.

Arai, S., Okamura, H., Kadoshima, K., Tanaka, C., Suzuki, K., and Ishimaru, S., 2011. Chemical characteristics of chromian spinel in plutonic rocks: implications for deep magma processes and discrimination of tectonic setting. *Island Arc*, 20 (1): 125–137.

Augé, T., 1986, Platinum-group mineral inclusions in chromitites from the Oman ophiolite. *Bull. Minéral.*, 109: 301–304.

Augé, T., 1987. Chromite deposits in the northwestern Oman ophiolite: mineralogical constraints. *Minerl. Deposita*, 22: 1–10.

Augé, T., Legendre, O., and Maurizot, P., 1998, The distribution of Pt and Ru-Os-Ir minerals in the New Caledonia ophiolite. In: Laverov, N. P., and Distler, V.V. (eds.), *International Platinum.* Athens: Theophrastus publications, 141–154.

Babaie, H.A., Ghazi, A.M., Babaie, A., La-Tour, T.E., and Hassanipak, A.A., 2000. Geochemistry of arc volcanic rocks of the Zagros crush zone, Neyriz, Iran. *J. Asian Earth Sci.*, 19 (1): 61–76.

Babien, J., Shallo, M., Mankia, K., and Gega, D., 1998. The Shebenik massif (Albania): a link between MORB and SSZ type Ophiolites. *Ofioliti*, 23: 7–15.

Bacuta, G.K., Kay, R.W., Gibbs, A.K., and Lipin, B.R., 1990. Platinum-group elements abundance in chromite deposits of the Acoje ophiolite block, Zambales ophiolite complex, Philippines. *J. Geochem. Exploration*, 37(1): 113–145.

Barnes, S.J., Naldrett, A.J., and Gorton, M.P., 1985. The origin of the fractionation of the platinum-group elements in terrestrial magmas. *Chemical Geol.*, 53: 303–323.

Barnes, S.J., and Roeder, P.L., 2001. The range of spinel compositions in terrestrial mafic and ultramafic rocks. *J. Petrology*, 42(12): 2279–2302.

Başpınar, G., 2006. Guleman (Elazığ) Bölgesi Krom Yataklarının Platin Grubu Element İçerikleri ve Jeokimyası. Fırat Üniversitesi, Fen Bilimleri Enstitüsü, Yüksek Lisans Tezi, 138 s (unpublished), Elazığ.

Berberian, M., and King, G.C.P., 1981. Towards a paleogeography and tectonic evolution of Iran. *Canadian J. Earth Sci.*, 18(2): 21–26.

Berberian, F., and Berberian, M., 1981. Tectono-plutonic episodes in Iran. In: Gupta, H.K., and Delany, F.M. (eds.), *Zagros-Hindu Kush-Himalaya Geodynamic Evolution*. American Geophysical Union, Geodynamic Series, 3: 5–32.

Bodinier, J.L., Vasseur, G., Vernieres, J., and Dupuy, C.F.J., 1990. Mechanisms of mantle metasomatism: geochemical evidence from the Lherz orogenic peridotite. *J. Petrology*, 31 (3): 597–628.

Bonavia, F.F., Diella, V., and Ferrario, A., 1993. Precambrian podiform chromitites from Kenticha Hill, southern Ethiopia. *Economic Geol.*, 88(1): 198–202.

Brenan, J.M., and Andrews, D., 2001. High temperature stability of laurite and Ru-Os-Ir alloy and their role in PGE fractionation in mafic magmas. *Canadian Mineral.*, 39(2): 341–360.

Bridges, J.C., Prichard, H.M., Meireles, C.A., 1995. Podiform chromitite-bearing ultrabasic rocks from the Braganca massif, northern Portugal: fragments of island arc mantle? *Geol. Mag.*, 132: 39–49.

Büchl, A., Brügmann, G., and Batanova, V.G., 2004. Formation of podiform chromitite deposits: implications from PGE abundances and Os isotopic compositions of chromites from the Troodos complex, Cyprus. *Chemical Geol.*, 208(1): 217–232.

Burgath, K.P., Krauss, U., and Mohr, M., 2002. Chromium ores and platinum-group-element occurrences in Europe and Turkey: inventory, evaluation and possibilities. Chronique de

la recherche minière, No hors série, 55–75.

Cameron, W.E., Mcculloch, M.T., and Walker, D.A., 1983. Boninite petrogenesis: chemical and Nd-Sr isotopic constraints. *Earth Planet. Sci. Lett.*, 65(1): 75–89.

Cameron, W.E., 1985. Petrology and origin of primitive lavas from the Troodos ophiolite, Cyprus. *Contribut. Mineral. Petrol.*, 89: 239–255.

Cassard, D., Nicolas, A., Rabinovitch, M., Moutte, J., Leblanc, M., and Prinzhofer, A., 1981. Structural classification of chromite pods in southern New Caledonia. *Economic Geol.*, 76 (4): 805–831.

Dare, S.A.S., Pearce, J.A., Mcdonald, I., and Styles M.T., 2008. Tectonic discrimination of peridotites using f_{O2}-Cr# and Ga-Ti -Fe^{III} systematics in chromian-spinel. *Chemical Geol.*, 261(3-4): 199−216.

Deschamps, F., Guillot, S., Godard, M., Chauvel, C., Andreani, M., and Hattori, K., 2010. In situ characterization of serpentinites from fore arc mantle wedges: timing of serpentinization and behavior of fluid-mobile elements in subduction zones. *Chemical Geol.*, 269(3−4): 262−277.

Dick, H.J.B., and Bullen, T., 1984. Chromian spinel as petrogenetic indicator in abyssal and Alpine-type peridotite and specially associated lavas. *Contribut. Mineral. Petrol.*, 86 (1): 54–76.

Dönmez, C., Keskin, S., Günay, K., Çolakoğlu, A.O., Çiftçi, Y., and Uysal, İ., 2014. Chromite and PGE geochemistry of the Elekdağ Ophiolite (Kastamonu, Northern Turkey): Implications for deep magmatic processes in a supra-subduction zone setting. *Ore Geol. Rev.*, 57(1): 216–228.

Droop, G.T.R., 1987. A general equation for estimating Fe^{3+} concentrations in ferromagnesian silicates and oxides from microprobe analyses, using stoichiometric criteria. *Mineral. Magazine*, 51(361): 431–435.

Economou-Eliopoulos, M., 1996. Platinum-group element distribution in chromite ores from ophiolite complexes: Implications for their exploration. *Ore Geol. Rev.*, 11: 363−381.

Economou-Eliopoulos, M., Eliopoulos, D.G., and Tsoupas, G., 2017. On the diversity of the PGE content in chromitites hosted in ophiolites and in porphyry-Cu systems: Controlling factors, *Ore Geol. Rev.*, 88: 156–173.

Fisk, M.R., and Bence, A.E., 1980. Experimental crystallization of chrome spinel in FAMUS basalt 527-1-1. *Earth Planet. Sci. Lett.*, 48(1):111–123.

Flower, M.F.J., and Levine, H.M., 1987. Petrogenesis of a tholeiite-boninite sequence from Ayios Mamas, Troodos ophiolite: Evidence for splitting of a volcanic arc? *Contribut. Mineral. Petrol.*, 97(4): 509−524.

Garuti, G., Zaccriani, F., Cabella, R., and Fershatater, G., 1997. Occurrence of unknown Ru-Os-Ir-Fe oxides in chromitite of Nurali-altramafic complex south of Urals, Russia. *Canadian Mineral.*, 35(6): 1431–1439.

Garuti, G., Fershtater, G., Bea, F., Montero, P., Pushkarev, E.V., and Zaccarini, F., 1997. Platinum-group elements as petrological indicators in mafic–ultramafic complexes of the central and southern Urals: preliminary results. *Tectonophysics*, 276(1−4): 181−194.

Garuti, G., 2004. Chromite-platinum-group element magmatic deposits. In: De Vivo, B., and Stüwe, K. (eds.), *Geology, Encyclopedia of Life Support Systems (EOLSS)*. UNESCO, EOLSS Publisher, Oxford (United Kingdom) (http://www.eolss.net).

Garuti, G., Pushkarev, E.V., and Zaccarini, F., 2005. Diversity of chromite-PGE mineralization in ultramafic complexes of the Urals. In: Törmänen, T.O., and Alapieti, T.T. (eds.), *Platinum-group Elements — From Genesis to Benefication and Environmental Impact*. Oulu (Finland), August 8–11, 10th International Platinum Symposium, Extended Abstracts, 341–344.

Gervilla, F., Proenza, J.A., Frei, J.M., Gonzales-Jimenez, C.J., Garrido, J.C., Melgajero, A., Meibon, A., Diaz-Martinez, R., and Lavaut, W., 2005. Distribution of platinum-group elements and Os isotopes in chromite ores from Mayari-Baracoa (eastern Cuba). *Contribut. Mineral. Petrol.*, 150(6): 589–607.

Ghazi, J.M., Moazzen, M., Rahgoshay, M., and Shafaii Moghadam, H., 2010. Mineral chemical composition and geodynamic significance of peridotites from Nain ophiolite, Central Iran. *J Geodynamics*, 49(5): 261–270.

Ghazi, J.M., Moazzen, M., Rahgoshay, M., and Shafaii Moghadam, H., 2011. The geodynamic setting of the Nain ophiolites, Central Iran: evidence from chromian spinels in the chromitites and associated rocks. *Ofioliti*, 36 (1): 59–76.

González-Jiménez, J.M., Kerestedjian, T., Proenza, J.A., and Gervilla, F., 2009. Metamorphismon chromite ores from the Dobromirtsi ultramafic massif, Rhodope Mountains (SE Bulgaria). *Geologica Acta*, 7 (4): 413–429.

González-Jiménez, J.M., Proenza, J.A., Gervilla, F.,Melgarejo, J.C., Blanco-Moreno, J.A., Ruiz- Sánchez, R., and Griffin, W.L., 2011. High-Cr and high-Al chromitites from the Sagua de Tánamo district, Mayarí-Cristal ophiolitic massif (eastern Cuba): constraints on their origin from mineralogy and geochemistry of chromian spinel and platinum-group elements. *Lithos*, 125(1): 101–121.

Grammatikopoulos, T.A., Kapsiotis, A., Tsikouras, B., Hatzipanagiotou, K., Zaccarini, F., and Garuti, G., 2011. Spinel composition, PGE geochemistry and mineralogy of the chromitites from the Vourinos ophiolite complex, Northwestern Greece. *Canadian Mineral.*, 49(6): 1571–1598.

Guolin, G., Jingsui, Y., Robinson, P.T., Xiaodong, L., Xianzhen, X., and Fahui, X., 2016. Platinum-group mineral (PGM) and base-metal sulphide (BMS) inclusions in chromitites of the Zedang Ophiolite, Southern Tibet, China and their petrogenetic significance. *Acta Geologica Sinica* (English Edition), 90 (3): 900–912.

Hamlyn, P.R., Keays, R.R., Cameron, W.E., Crawford, A.J., and Waldron, H.M., 1985. Precious metals in magnesian low-Ti lavas: implications for metallogenesis and sulphur saturation in primary magmas. *Geochim. Cosmochim. Acta*, 49(8): 1797–1811.

Hamlyn, P.R., and Keays, R.R., 1986. Sulfur saturation and second stage melts: application to the Bushveld Pt metal deposits. *Economic Geol.*, 81(6): 1431–1445.

Haynes, S.J., and Reynolds, P.H., 1980. Early development of Tethys and Jurassic ophiolite displacement. *Nature*, 283: 560–563.

Habtoor, A.M., Ahmed, A.H., Akizawa, N., Harbi, H., and Arai, S., 2017. Chemical homogeneity of high-Cr chromitites as indicator for widespread invasion of boninitic melt in mantle peridotite of Bir Tuluha ophiolite, Northern Arabian Shield, Saudi Arabia. *Ore Geol. Rev.*, doi.org/10.1016/j.oregeorev.2017.03.010.

Huang, X., Li, J., Kusky, T.A., and Chen, Hz., 2004. Microstructures of the zunhua 2.50 ga podiform chromite, north china craton and implications for the deformation and rheology of the archean oceanic lithospheric mantle. *Precambrian Ophiolites Related Rocks Developments Precambrian Geol.,* 13: 321–338.

Imamali Pour, A., 2011. Geochemistry and geological environment of the Elendaz chromitite, Khoy ophiolite, northwest of Iran. *Earth Sci.*, 8(1): 47–56.

Irvine, T.N., 1967. Chromian spinel as a petrogenetic indicator. Part 2, petrologic applications theory. *Canadian J. Earth Sci.*, 4(1): 71–103.

Irvine, T.N., 1975. Crystallization sequences in the Muskox intrusion and other layered intrusions-II. Origin of chromitite layers and similar deposits of other magmatic ores. *Geochim. Cosmochim. Acta*, 39(6): 991–1020.

Irvine, T.N., 1977. Origin of chromite layers in the Muskox intrusion and other intrusions: a new interpretation. *Geology*, 5 (5): 273–277.

Ismail, S.A., Mirza, T.M., and Carr, P.F., 2010. Platinum-group elements geochemistry in podiform chromitites and associated peridotites of the Mawat ophiolite, northeastern Iraq. *J. Asian Earth Sci.*, 37(1): 31–41.

Ismail, S.A., Kettanah, Y.A., Chalabi, S.N., Ahmed, A.H., and Arai, S., 2014. Petrogenesis and PGE distribution in the Al- and Cr-rich chromitites of the Qalander ophiolite, northeastern Iraq: Implications for the tectonic environment of the Iraqi Zagros Suture Zone. *Lithos*, 202–203: 21–36.

Ishikawa, V.S., Crawford, A.J., and Meffre, S., 2001. Factors controlling chemistry of magmatic spinel: An empirical study of associated olivine, Cr-spinel and melt inclusions from primitive rocks. *J. Petrol.*, 42(4): 655−671.

Ishikawa, T., Nagaishi, K., and Umino, S., 2002. Boninitic volcanism in the Oman ophiolite: implications for thermal condition during transition from spreading ridge to arc. *Geology*, 30(10): 899–902.

Jannessary, M.R., Melcher, F., Lodziak, J., and Meisel, T.C., 2012. Review of platinum-group element distribution and mineralogy in chromitite ores from southern Iran. *Ore Geol. Rev.*, 48(1): 278–305.

Jaavid, Z., 2012. Textural and geochemical studies of the Cheshmeh-Bid chromite deposit (NW-Neyriz, Fars Province). Unpublished M.Sc. thesis, Urumieh University, Iran, 178.

Jenner, G.A., 1981. Geochemistry of high-Mg andesites from Cape Vogel, Papua New Guinea. *Chemical Geol.*, 33(1–4): 307–332.

Kamenetsky, V.S., Crawford, A.J., and Meffre, S., 2001. Factors controlling chemistry of magmatic spinel: an empirical study of associated olivine, Cr-spinel and melt inclusions from primitive rocks. *J. Petrol.*, 42(2): 655–671.

Kamenetsky, V.S., Sobolev, A.V., Eggins, S.M., Crawford, A.J., and Arculus, R.J., 2002. Olivineenriched melt inclusions in chromites from low-Ca boninites, Cape Vogel, Papua New Guinea: evidence for ultramafic primary magma, refractory mantle source and enriched components. *Chemical Geol.*, 183 (1–4): 287–303.

Karipi, S., Tsikouras, B., and Hatzipanagiotou, K., 2006. The petrogenesis and tectonic setting of ultramafic rocks from Iti and Kallidromon Mountains, continental Central Greece: vestiges of the Pindos Ocean. *Canadian Mineral.*, 44(1): 267–287.

Kelemen, P.B., Joyce, D.B., Webster, J.D., and Holloway, J.R., 1990. Reaction between ultramafic rock and fractionating basaltic magma II. Experimental investigation of reaction between olivine tholeiite and harzburgite at 1150°−1050°C and 5 Kb. *J. Petrol.*, 31(1): 99−134.

Kelemen, P.B., Dick, H.J.B., and Quick, J.E., 1992. Formation of harzburgite by pervasive melt/rock interaction in the upper mantle. *Nature,* 358: 635–641.

Kocks, H., Melcher, F., Meisel, T., and Burgath, K.P., 2007. Diverse contributing sources to chromitite petrogenesis in the Shebenik ophiolitic complex, Albania: evidence from new PGE-and Os-isotope data. *Mineral. Petrol.,* 91: 139–170.

Kozlu, H., Prichard, H., Melcher, F., Fisher, P., Brough, C., and Stueben, D., 2014. Platinum-group element (PGE) mineralisation and chromite geochemistry in the Berit ophiolite (Elbistan/Kahramanmaraş), SE Turkey. *Ore Geol. Rev.*, 60: 97–111.

Leblanc, M., and Violette, J.F., 1983. Distribution of aluminium-rich and chromium-rich chromite pods in ophiolite peridotites. *Economic Geol.*, 78(2): 293–301.

Le Mee, L., Girardeau, J., and Monnier, C., 2004. Mantle segmentation along the Oman ophiolite fossil mid-ocean ridge. *Nature,* 432: 167–172.

Lipin, B.R., 1993. Pressure increases in the formation of chromite seams and the development of the ultramafic series in the Stillwater complex, Montana. *J. Petrol.*, 34(5): 955–976.

Malitch, K.N., Thalhammer, O.A.R., Knauf, V.V., and Melcher, F., 2003. Diversity of platinum-group mineral assemblages in an Eastern Alpine ophiolite: a case study of banded and podiform chromitite from the Kraubath ultramafic massif, Austria. *Mineral. Deposita*, 38(3): 282–297.

Maurel, C., and Maurel, P., 1982. Étude expérimentale de la distribution de l'aluminium entre bain silicaté basique et spinelle chromifère. Implications pétrogénétiques: teneur en chromian des spinelles. *Bull. Minéral.*, 105: 197−202.

Maurel, C., and Maurel, P., 1983. Influence du fer ferrique sur la distribution de l'aluminium entre bain silicaté basique et spinelle chromifère. *Bull. Minéral.*, 106: 623–624.

Maurel, C., 1984. *Etude expdrimentale de l'rquilibre spinelle chromif'ere liquide silicate basique*. SFMC Meet. "Les spinelles", Lille, oral. comm, (cited in Auge, 1987).

McDonough, W.F., and Sun, S., 1995. The composition of the Earth. *Chemical Geol.*, 120(3–4): 223–253.

Mcelduff, B., and Stumpfl, E.F., 1990. Platinum-group minerals from Troodos ophiolite, Cyprus. *Mineral. Petrol.,* 42(1): 211–232.

Melcher, F., Grum, W., Simon, G., Thalhammer, T.V., and Stumpfl, F.E., 1997. Petrogenesis of the ophiolitic giant chromite deposits of Kempirsai, Kazakhstan: a study of solid and fluid inclusions in chromite. *J. Petrol.*, 38(3): 1419–1438.

Melcher, F., Grum, W., Thalhammer, T. V., and Thalhammer, O.A.R., 1999. The giant chromite deposit at Kempirsai, Ural; constraints from trace elements (PGE, REE) and isotope data. *Mineral. Deposita*, 34(3): 250–272.

Moafpourian, G., Vosoghi Abedini, M., Emami, M., Janessari, M., and Parmen, S., 2010. Investigation of petrogenesis of ultramafic- mafic rocks, East Fariman, Northeast Iran. *Earth Sci.*, 18: 24–11.

Mukasa, S., and Ludden, J.N., 1987. Uranium-lead isotopic ages of plagiogranites from the Troodos ophiolite, Cyprus, and their tectonic signifi cance. *Geology*, 15: 825–828.

Mungall, J.E., 2005, Magmatic geochemistry of the platinum-group elements. In: Mungall, J.E. (ed.), *Exploration for Platinum-group Element Deposits*. Mineralogical Association of Canada, Short Course Series, 35(1): 1–34.

Mysen, B.O., and Kushiro, I., 1977. Compositional variations of coexisting phases with degrees of melting of peridotite in the upper mantle. *American Mineral.*, 62(1): 843−865.

Najafzadeh, A.R., Arvin, M., Pan, Y., and Ahmadipour. H., 2008. Podiform Chromitites in the Sorkhband Ultramafic Complex, Southern Iran: Evidence for Ophiolitic Chromitite. *J. Sci. Islamic Republic Iran*, 19(1): 49–65.

Najafzadeh, A. R., and Ahmadipour, H., 2016. Geochemistry of platinum-group elements and mineral composition in chromitites and associated rocks from the Abdasht ultramafic complex, Kerman, Southeastern Iran, *Ore Geol. Rev.,* 75: 220–238.

Naldrett, A.J., Hoffman, E.L., Green, A.H., Chou, C.L., Naldrett, S.R., and Alcock, R.A., 1979. the composition of Ni-sulfide ores with particular reference to their content of PGE and Au. *Canadian Mineral.*, 17(2): 403–415.

Naldrett, A.J., and Duke, J.M., 1980. Platinum metals in magmatic sulfide ores. *Science,* 208(4451): 1417–1424.

Naldrett, A.J., and Von Gruenewaldt, G., 1989. Association of platinum-group elements with chromitite in layered intrusions and ophiolite complexes. *Economic Geol.*, 84(1): 180–187.

O'Hara, M.J., Fry, N., and Prichard, H.M., 2001a, Minor phases as carriers of trace elements in non-modal crystal-liquid separation processes I: Basic relationships. *J. Petrol.*, 42(10): 1869–1885.

O'Hara, M.J., Fry, N., and Prichard, H.M., 2001b, Minor phases as carriers of trace elements in non-modal crystalliquid separation processes II: illustrations and bearing on behavior of REE, U, Th and PGE in igneous processes. *J. Petrol.*, 42 (10): 1887–1910.

Ohnenstetter, M., Karaj, N., Neziraj, A., Johan, Z., and Cina, A., 1991. Le potential platinifère des ophiolites: minéralisations en éléments du groupe de platine (PGE) dans les massifs de Tropoja et Bulqiza, Albanie. C. R. Acad. Sci. Paris 313 (Série II): 201–208.

Okamura, H., Arai, S., and Kim, Y.U., 2006. Petrology of forearc peridotite from the Hahajima Seamount, the Izu-Bonin arc, with special reference to chemical characteristics of chromian spinel. *Mineral. Magazine*, 70: 15–26.

Orberger, B., Lorand, J.P., Girardeau, J., Mercier, J.C.C., and Pitragool, S., 1995. Petrogenesis of ultramafic rocks and associated chromitites in the Nan Uttaradit ophiolite, Northern Thailand. *Lithos,* 35(3–4): 153–182.

Pagé, P., and Barnes, S.J., 2009. Using Trace Elements in Chromites to Constrain the Origin of Podiform Chromitites in the Thetford Mines Ophiolite, Québec, Canada. *Economic Geol.*, 104(7): 997–1018.

Pagé, P., Bédard, J.H., Schroetter, J.M., and Tremblay, A., 2008. Mantle petrology and mineralogy of the Thetford Mines Ophiolite Complex. *Lithos*, 100(2): 255−292.

Paktunc, A.D., and Cabri, L.J., 1995. A proton- and electron-microprobe study of gallium, nickel and zinc distribution in chromian spinel. *Lithos*, 35(3–4): 261–282.

Pal, T., 2011. Petrology and geochemistry of the Andaman ophiolite: melt-rock interaction in a suprasubduction-zone setting. *J. Geol. Soc. London,* 168(4): 1031–1045.

Parkinson, I.J., and Pearce, J.A., 1998. Peridotites from the Izu-Bonin-Mariana forearc (ODP Leg 125): evidence for mantle melting and melt-mantle. *J. Petrol*, 39(9): 1577–1618.

Peighambari, S., Uysal, I., Stosch, H. G., Ahmadipour, H., and Heidarian, H., 2016. Genesis and tectonic setting of ophiolitic chromitites from the Dehsheikh ultramafic complex (Kerman, southeasternIran): Inferences from platinum-group elements and chromite compositions, *Ore Geol. Rev.*, 74: 39–51.

Prichard, H.M., Puchelt, H., Eckhardt, J.D., and Fisher, P.C., 1996. Platinum-group element concentrations in mafic and ultramafic lithologies drilling from Hess Deep. In: M'evel, C. et al. (eds.). Proceeding Ocean Drilling Program. *Sci. Res.,* 147: 77–90.

Prichard, H.M., Neary, C.R., Fisher, P.C., and O'hara, M.J., 2008. PGE-rich podiform chromitites in the Al 'Ays Ophiolite Complex, Saudi Arabia - An example of critical mantle melting to extract and concentrate PGE. *Economic Geol.*, 103 (7): 1507–1529.

Proenza, J.A, Gervilla, F., Melgarejo, J.C, and Bodinier J.L., 1999. Al- and Cr-rich chromitites from the Mayarí-Baracoa Ophiolitic Belt (Eastern Cuba): consequence of interaction between volatile-rich melts and peridotites in suprasubduction mantle. *Economic Geol.*, 94(4): 547–566.

Proenza, J.A., Zaccarini, F., Lewis, J.F., Longo, F., and Garuti, G., 2007. Chromian spinel composition and the platinum-group minerals of the PGE-rich Loma Peguera chromitites, Loma Caribe peridotite, Dominican Republic. *Canadian Mineral.*, 45: 631−648.

Rajabzadeh, M.A., Ohnenstetter, R.M., Ohnenstetter, D., and Reisberg, L., 1998. Chromian and platinum-group element (PGE) mineralization in chromitites from the Assemion and Neyriz ophiolites, Zagros Belt, Iran. 8th International Platinum Symposium abstracts, The Geological Society of South Africa and The South African Institute of Mining and Metallurgy Symposium Series S18: 343–345.

Rajabzadeh, M. A., Nazari Dehkordi, T., and Caran, S., 2013. Mineralogy, geochemistry and geotectonic significance of mantle peridotites with high-Cr chromitites in the Neyriz ophiolite from the outer Zagros ophiolite belts, Iran. *J. African Earth Sci.*, 78(1): 1–15.

Rehkämper, M., Halliday, A.N., Fitton, J.G., Lee, D.C., Wieneke, M., and Arndt, N.T., 1999. Ir, Ru, Pt, and Pd in basalts and komatiites: new constraints for the geochemical behavior of the platinum-group elements in the mantle: *Geochim.Cosmochim. Acta,* 63(22): 3915–3934.

Ricou, L.E., 1976. Evolution structurale des Zagrides. La region clef de Neyriz (Zagros Iranien). - Memoire Societé Geologie De La France, 140.

Ricou, L.E., Braud, J., and Brunn, J.H., 1977. Le Zagros. *Société Géologique de France, Mémoire Hors-Série*, 8(2): 33–52.

Robertson, A.H.F., 2002, Overview of the genesis and emplacement of Mesozoic ophiolites in the Eastern Mediterranean Tethyan region: *Lithos*, 65(1): 10–67.

Robinson, P., T., Zhue, M., F., Malpas, J., and Wen J.B., 1997. Podiform chromitites: their composition, origin and environment of formation. *Episodes*, 4: 247–252.

Robinson, P.T., Zhou, M.F., 2008. The origin and tectonic setting of ophiolites in China. *Journal of Asian Earth Sciences*, 32(5–6): 301–307.

Robinson, P.T., Trumbull, R.B., Schmitt, A., Yang, J.S., Li, J.W., Zhou, M.F., Erzinger, J., Sarah Dare, S., and Xiong, F.,

2015. The origin and significance of crustal minerals in ophiolitic chromitites and peridotites. *Gondwana Res.*, 27(2): 486–506.

Roeder, P.L., and Reynolds, I., 1991. Crystallization of chromite and chromium solubility in basaltic melts. *J. Petrol.*, 32(5): 909–934.

Rollinson, H., 2005. Chromite in the mantle section of the Oman ophiolite: a new genetic model. *Island Arc,* 14(4): 542–550.

Rollinson, H., 2008. The geochemistry of mantle chromitites fromthe northern part of the Oman ophiolite: inferred parental melt compositions. *Contribut. Mineral. Petrol.,* 156(3): 273–288.

Sarkarinejad, K., 2003. Structural and microstructural analysis of a palaeotransform fault zone in the Neyriz ophiolite, Iran. In: Dilek, Y., and Robinson, R.T. (eds.), *Ophiolite in Earth History*. The Geological Society of London, Special Publications, 218: 129–145.

Schroetter, J.-M., Tremblay, A., and Bédard, J.H., 2005. Structural evolution of the Thetford-Mines Ophiolite Complex, Canada, and its implications for origin of the southern Québec ophiolitic belt. *Tectonics*, 24(1): TC1001, 20.

Scowen, P.A.H., Roeder, P.L., and Helz, R.T., 1991. Reequilibration of chromite within Kilauea Iki lava lake, Hawaii. *Contribut. Mineral. Petrol.,* 107(1): 8–20.

Shafaii Moghadam, H., Rahgoshay, M., and Forouzesh, V., 2009. Geochemical investigation of nodular chromites in the Forumad ophiolite, NE of Iran. *Iranian J. Sci. Tech., Transaction*, 33(3): 1–18.

Shafaii Moghadam, H., Stern, R.J., and Rahgoshay, M., 2010. The Dehshir ophiolite (central Iran): Geochemical constraints on the origin and evolution of the Inner Zagros ophiolite belt. *GSA Bull.*, 122(9–10): 1516–1547.

Shafaii Moghadam, H., and Stern, R.J., 2011a. Geodynamic evolution of Upper Cretaceous Zagros ophiolites: formation of oceanic lithosphere above a nascent subduction zone. *Geol. Magazine,* 148(5–6): 762–801.

Shafaii Moghadam, H., and Stern, R.J., 2011b. Late Cretaceous forearc ophiolites of Iran. Island Arc 20, 1– .4Economou-Eliopoulos, M., 1996. Platinum-group elements distribution in chromite ores from ophiolite complexes: implications for their exploration. *Ore Geol. Rev.,* 11: 363–381.

Shafaii Moghadama, H., Khedrb, M.Z., Chiaradiad, M., Sterne, R.J., Bakhshizada, F., Araib, Sottleyf, C.J., and Tamurab, A., 2014. Supra-subduction zone magmatism of the Neyriz ophiolite, Iran: constraints from geochemistry and Sr-Nd-Pb isotopes. *Intl Geol. Rev.*, 56(11): 1395–1412.

Shafaii Moghadam, H., Zaki Khedr, M., Arai, S., Stern, R.J., Ghorbani, G., Tamura, A., and Ottley, C.J., 2015. Arc-related harzburgite-dunite-chromitite complexes in the mantle section of the Sabzevar ophiolite, Iran: A model for formation of podiform chromitites. *Gondwana Res.*, 27(2): 575–593.

Shahabpour, J., 2005. Tectonic evolution of the orogenic belt in the region located between Kerman and Neyriz. *J. Asian Earth Sci.*, 24(4): 405–417.

Shen-Su, S., 1982. Chemical composition and origin of the earth's primitive mantle, *Geochim. Cosmochim. Acta*, 46(2): 179–192.

Soleimani, M., and Jodeiri Shokri, B., 2016. Intrinsic geological model generation for chromite pods in the Sabzevar ophiolite complex, NE Iran. *Ore Geol. Rev.*, 78: 138–150.

Stocklin, J., 1974. Possible ancient continental margin in Iran. In: Burk, C.A., and Drake, C.L. (eds.): *The Geology of Continental Margins*, Berlin: Springer, 873–887.

Taghipour, B., Nejadhadad, M., Mackizadeh, M.A., Noghreian, M., and Rahimi, P., 2015. Using mineralogy and geochemistry of Cheshmeh-Bid chromitites (Neyriz) for determination of tectonic setting, Scientific *Quarterly J. Geosci.*, 95(3): 63–74.

Tamura, A., and Arai, S., 2006. Harzburgite-dunite-orthopyroxenite suite as a record of suprasubduction zone setting for the Oman ophiolite mantle. *Lithos,* 90(1–2): 43–52.

Thayer, T.P., 1964. Principle features and origin of podiform chromite deposits and some observations on the Guleman-Soridag district, Turkey. *Economic Geol.*, 59(8): 1497–1524.

Uysal, I., Sadiklar, M.B., Tarkian, M., Karsli, O., and Aydin, F., 2005. Mineralogy and composition of the chromitites and their platinum-group minerals from Ortaca (Mugla-SW Turkey): Evidence for ophiolitic chromitite genesis: *Mineral. Petrol.*, 83 (3): 219−242.

Uysal, I., Tarkian, M., Sadiklar, M.B., and Sen, C., 2007. Platinum-group-element geochemistry and mineralogy of ophiolitic chromitites from the Kop Mountains, northeastern Turkey. *Canadian Mineral.*, 45: 355−377.

Uysal, I., Tarkian, M., Sadiklar, M.B., Zaccarini, F., Meisel, T., Garuti, G., and Heidrich, S., 2009. Petrology of Al- and Cr-rich ophiolitic chromitites from the Muğla, SW Turkey: implications from composition of chromite, solid inclusions of platinum-group mineral, silicate, and base-metal mineral, and Os-isotope geochemistry. *Contribut. Mineral. Petrol.*, 158(5): 659–674.

Walker, D.A., and Cameron, W.E., 1983. Boninite primary magmas: evidence from the Cape Vogel Peninsula, PNG. *Contribut. Mineral. Petrol.,* 83(1): 150–158.

Xiong, F.H., Yang, J.S., Robinson, P.T., Xu, X.Z., Liu, Z., Li, Y., Liu, F., and Chen, S.Y., 2015a. Origin of podiform chromitite, a new model based on the Luobusa ophiolite, Tibet. *Gondwana Res.,* 27(2): 525–542.

Xiong, F.H., Yang, J.S., Robinson, P.T., Dilek, Y., Milushi, I., Xu, X.Z., Chen, Y.H., Zhou, W.D., Zhang, Z.M., Lai, S.M., Tian, Y.Z., and Huang, Z., 2015b. Petrology and geochemistry of high Cr# podiform chromitites of Bulqiza, Eastern Mirdita Ophiolite (EMO), Albania. *Ore Geol. Rev.,* 70: 188–207.

Xiong, F., Yang, J., Robinson, P. T., Xu, X., Liu, Z., Zhou, W., Feng, G., Xu, J., Li, J., and Niu, X., 2017. High-Al and high-Cr podiform chromitites from the western Yarlung-Zangbo suture zone, Tibet: Implications from mineralogy and geochemistry of chromian spinel, and platinum-group elements. *Ore Geol. Rev.*, 80: 1020–1041.

Xu, X.Z., Yang, J.S., Robinson, P.T., Xiong, F.H., Ba, D.Z., and Guo, G.L., 2015. Ultrahigh pressure, highly reduced and crustal-type minerals from podiform chromitite and mantle peridotite of the Luobusa ophiolite, Tibet. *Gondwana Res.*, 27 (2): 686–700.

Yaghubpur, A., 2005. Mineral deposits of Iran: a brief review. In: Roonwal, G.S., Shahriar, K., and Ranjbar, H. (eds.), *Mineral Resources and Development*. Daya Publishing House, Delhi-110 035: 191–202.

Yang, J., Meng, F., Xu, X., Robinsona, P.T., Dilek, Y., Alexander B. Makeyev, A.B., Wirth, R., Wiedenbeck, M., and Cliff, J., 2015. Diamonds, native elements and metal alloys from chromitites. *Gondwana Res.*, 27(2): 459–485.

Zaccarini, F., Garuti, G., Proenza, J.A., Campos, L., Thalhammer, O.A.R., Aiglsperger, T., and Lewis, J., 2011.

Chromite and platinum-group-elements mineralization in the Santa Elena ophiolitic ultramafic nappe (Costa Rica): geodynamic implications. *Geologica Acta,* 9(3–4): 407–423.

Zaeimnia, F., Arai, S., and Mirmohammadi, M., 2017. Na-rich character of metasomatic/metamorphic fluids inferred from preiswerkite in chromitite pods of the Khoy ophiolite in Iran: Role of chromitites as capsules of trapped fluids, *Lithos*, 268–271: 351–363.

Zhou, M.F., and Bai, W.J., 1992. Chromite deposits in China and their origin. *Mineral. Deposita,* 27(3): 192–199.

Zhou, M.F., and Bai, W.J., 1994. Formation of podiform chromitites by melt/rock interaction in the upper mantle. *Mineral. Deposita,* 29(1): 98–101.

Zhou, M.F., and Robinson, P.T., 1994. High-Cr and high-Al podiform chromitites, western China: Relationship to partial melting and melt/rock reaction in the upper mantle. *International Geol. Rev.,* 36: 678−686.

Zhou, M.F., Robinson, P.T., Malpas, J., and Li, Z., 1996. Podiform chromitites in the Luobusa ophiolite (Southern Tibet): implications for melt-rock interaction and chromite segregation in the upper mantle. *J. Petrol.,* 37(1): 3–21.

Zhou, M.F., and Robinson, P.T., 1997. Origin and tectonic setting of podiform chromite deposits. *Economic Geol.,* 92(2): 259–262.

Zhou, M.F., Sun, M., Keays, R.R., and Kerrich, R.W., 1998. Controls on platinum-group elemental distributions of podiform chromitites: a case study of high-Cr and high-Al chromitites from Chinese orogenic belts. *Geochim. Cosmochim. Acta,* 62(4): 677–688.

Zhou, M.F., Robinson, P.T., Malpas, J., Aitchison, J., Sun, M., Bai, W.J., Hu, X.F., and Yang, J.S., 2001. Melt/mantle interaction and melt evolution in the Sartohay high-Al chromite deposits of the Dalabute ophiolite (NW China). *J. Asian Earth Sci*., 19(4): 517–534.

Zhou, M.-F., Robinson, P.T., Malpas, J., Edwards, S.J., and Qi, L., 2005. REE and PGE geochemical constraints on the formation of dunites in the Luobusa ophiolite, Southern Tibet. *J. Petrol*., 46: 615–639.

About the first author

Batoul TAGHIPOUR was born in Isfahan City. She is the Assistant Professor of petrology and geochemistry at the Shiraz University, Shiraz. She conducts research into igneous petrology, geochemistry, and economic geology and has published about 50 papers in the field of the MVT deposits, igneous petrology and geochemistry of modern continental rifts, bauxite deposits, mineral chemistry and evolution of tectonomagmatic processes. Email: Taghipour@shirazu.ac.ir; phone: +98 917 409 1677.